DEPARTMENT OF PHYSICS
UNIVERSITY OF JYVÄSKYLÄ
RESEARCH REPORT No. 11/2015

# SPECTRAL ANALYSIS AND QUANTUM CHAOS IN TWO-DIMENSIONAL NANOSTRUCTURES

BY

PERTTU LUUKKO

Academic Dissertation
for the Degree of
Doctor of Philosophy

To be presented, by permission of the
Faculty of Mathematics and Natural Sciences of the
University of Jyväskylä, for public examination in
Auditorium FYS1 of the University of Jyväskylä on
December 18, 2015, at noon

Jyväskylä, Finland
December 2015

ISBN 978-951-39-6375-0 (paper copy)
ISBN 978-951-39-6376-7 (electronic version)
ISSN 0075-465X

**Author** Perttu Luukko
Department of Physics
Nanoscience Center
University of Jyväskylä
Jyväskylä, Finland

**Supervisor** Prof. Esa Räsänen
Department of Physics
Tampere University of Technology
Tampere, Finland

**Reviewers** Dr. Tech. Ari Harju
Department of Applied Physics
Aalto University School of Science
Espoo, Finland

Prof. Matti Alatalo
Department of Physics
University of Oulu
Oulu, Finland

**Opponent** Prof. Jan Michael Rost
Max Planck Institute for the Physics of Complex Systems
Dresden, Germany

## Abstract

This thesis describes a study into the eigenvalues and eigenstates of two-dimensional (2D) quantum systems. The research is summarized in four scientific publications by the author. The underlying motivation for this work is the grand question of *quantum chaos*: how does chaos, as known in classical mechanics, manifest in quantum mechanics? The search and analysis of these quantum fingerprints of chaos requires efficient numerical tools and methods, the development of which is given a special emphasis in this thesis.

The first publication in this thesis concerns the eigenspectrum analysis of a nanoscale device. It is shown that a measured addition energy spectrum can be explained by a simple confinement of interacting electrons in a potential well. This result is derived using density-functional theory (DFT) and numerical optimization, guided by the asymmetric geometry of the device. The calculations also show that an observed decrease in the conductance can be explained by a change in the shape of the quantum wave function.

The study of quantum chaos by statistical properties of eigenvalues requires a way to solve the eigenvalue spectrum of a quantum system up to highly excited states. The second publication describes a numerical program, `itp2d`, that uses modern advances in the imaginary time propagation (ITP) method to solve the eigenvalue spectrum of generic 2D systems up to thousands of eigenstates. The program provides means to sophisticated eigenvalue analysis involving long-range correlations, and a unique view to highly excited eigenstates of complicated 2D systems, such as those involving magnetic fields and strong disorder.

After the spectrum is solved, the next step in the eigenvalue analysis is to remove the trivial part of the spectrum in a process known as unfolding. Unless the system belongs to a special class for which the trivial part is known, unfolding is an ambiguous process that can cause substantial artifacts to the eigenvalue statistics. Recently it has been proposed that these artifacts can be mitigated by employing the empirical mode decomposition (EMD) algorithm in the unfolding. The third publication describes an efficient implementation of this algorithm, which is also highly useful in other kinds of data analysis.

Quantum scarring refers to the condensation of quantum eigenstate probability density around unstable classical periodic orbits in chaotic systems. It represents a useful and visually striking quantum suppression of chaos. The final publication describes the discovery of a new kind of quantum scarring in symmetric 2D systems perturbed by local disorder. These unusually strong quantum scars are not explained by ordinary scar theory. Instead, they are caused by classical resonances and resulting quantum near-degeneracy in the unperturbed system. Wave-packet analysis shows that the scars greatly influence the transport properties of these systems, even to the extent that wave packets launched along the scar path travel with higher fidelity than in the corresponding unperturbed system. This discovery raises interesting possibilities of selectively enhancing the conductance of quantum systems by adding local perturbations.

## List of Publications

The results presented in this thesis are published in the following articles:

[I] K. Shibata, K. Seki, P. J. J. Luukko, E. Räsänen, K. M. Cha, I. Horiuchi, and K. Hirakawa, "Electronic structures in single self-assembled InAs quantum dashes detected by nanogap metal electrodes", Appl. Phys. Lett. **99**, 182104 (2011).

[II] P. J. J. Luukko and E. Räsänen, "Imaginary time propagation code for large-scale two-dimensional eigenvalue problems in magnetic fields", Comput. Phys. Commun. **184**, 769 (2013), arXiv:1311.1355 [physics.comp-ph]. Minor correction in: Comput. Phys. Commun. **198**, 262 (2016).

[III] P. J. J. Luukko, J. Helske, and E. Räsänen, "Introducing `libeemd`: a program package for performing the ensemble empirical mode decomposition", Comput. Stat. (2015) 10.1007/s00180-015-0603-9.

[IV] P. J. J. Luukko, B. Drury, A. Klales, L. Kaplan, E. J. Heller, and E. Räsänen, "Strong quantum scarring by random impurities", Phys. Rev. Lett. (2015), arXiv:1511.04198 [quant-ph], submitted.

The author designed and performed the numerical analysis in Publication I. Publications II and III describe programs codes that were designed and written by the author, except for the R interface in Publication III. In Publication IV, the author performed the numerical calculations and participated in the development of the theory. The initial drafts of Publications II, III, and IV were written primarily by the author.

During this thesis project the author has also taken part in the following publications:

[5] J. Solanpää, P. J. J. Luukko, and E. Räsänen, "Many-particle dynamics and intershell effects in Wigner molecules", J. Phys.: Condens. Matter **23**, 395602 (2011).

[6] J. Solanpää, J. Nokelainen, P. J. J. Luukko, and E. Räsänen, "Coulomb-interacting billiards in circular cavities", J. Phys. A: Math. Theor. **46**, 235102 (2013), arXiv:1210.2811 [nlin.CD].

[7] K. Shibata, N. Pascher, P. J. J. Luukko, E. Räsänen, S. Schnez, T. Ihn, K. Ensslin, and K. Hirakawa, "Electron magneto-tunneling through single self-assembled InAs quantum dashes", Appl. Phys. Express **7**, 045001 (2014).

[8] J. Solanpää, P. J. J. Luukko, and E. Räsänen, "Bill2d – a software package for classical two-dimensional Hamiltonian systems", Comput. Phys. Commun. **199**, 133 (2016), arXiv:1506.06917 [physics.comp-ph].

# Contents

# List of Figures

# Conventions

Numerical values and mathematical formulas in this thesis are given, unless explicitly specified otherwise, in the natural units of the Schrödinger equation. In these units, the mass of the studied particle $m = 1$, its charge $q = 1$, the Dirac constant $\hbar = 1$ and the Coulomb constant $1/4\pi\varepsilon_0 = 1$. In the context of electrons, these units are known as Hartree atomic units. As a result of the choice of units, many expressions are simplified. For example, the Hamiltonian of an electron in the hydrogen atom is

$$H = -\frac{1}{2}\nabla^2 + \frac{1}{r}.$$

# Preface

Before starting the introduction, several giants deserve thanks and acknowledgments for allowing me to stand on their shoulders.

First of all, I wish to thank my supervisor Esa Räsänen for his constant support and encouragement, and for teaching me various tricks of the trade that are useful in the busy life of the modern scientist. Despite surprises prepared for us by the forces of Chaos, it appears our explorations produced results that can be presented in a thesis. During my thesis projects I've also had the pleasure of collaborating with many other exceptional physicists; Ville Kotimäki, Janne Solanpää, Kenji Shibata, Byron Drury, Anna Klales, Lev Kaplan, and Eric Heller, to name a few.

Naturally I am indebted to the Department of Physics at the University of Jyväskylä for training and nurturing me for many years. Its professors have been a constant inspiration both in physics and in physical prowess, and its outstanding administrators, such as the *amanuensis emerita* Soili Leskinen, have made sure that everything works as smoothly and swiftly as University rules permit.

I also wish to thank the professors and teachers at the Department of Mathematics. I would be a lesser physicist without their training. Regarding mathematics, I am grateful to Markku Halmetoja for first showing me the enormous difference between mathematics and calculating.

During my time at the Department of Physics I've had the privilege of being part of the magnificent Holvi community at room YFL 353. Truly there has never been another band of colleagues quite like it. May its biannual conference cruises continue until the Sun boils the oceans.

In addition to the University of Jyväskylä, financial support for this work has been kindly provided by the Finnish Cultural Foundation, the Finnish Academy, the Emil Aaltonen Foundation, and the Magnus Ehrnrooth Foundation.

I am grateful to my parents for fueling my inclination to science, and my parents-in-law for their invaluable practical support during the recent years. Last, but certainly not the least, I wish to thank my wife Saila, my son Lauri, and my daughter Iiris for distracting me from the world of numbers with things that have true value.

Jyväskylä, December 9, 2015

Perttu Luukko

# Chapter 1

# Introduction

## 1.1 Chaos and classical dynamics

Chaos is a powerful word. Its original meaning is the primal void, a formless state that precedes the creation of the Universe. In ancient mythology and modern fiction alike chaos is a hostile, destructive force – a natural enemy or *order*, an embodiment of human reasoning. In science, chaos has a more specific and less sinister meaning, but a certain aura of mystique continues to surround the subject.

In a scientific context, chaos represents *unpredictability*. More specifically, it describes evolution in time that is fully deterministic, but still practically unpredictable due to extreme sensitivity to initial conditions. In a famous metaphorical example by E. N. Lorenz, the flap of a butterfly's wings can change the course of a hurricane occurring a few weeks later. A mathematically rigorous definition of chaos is a more complicated matter that is still discussed today[10], but for purpose of this introduction such definitions are unnecessary details[1].

Before the 20th century, chaos did represent a kind of a primal void that manifested in "unsolvable" systems such as the three-body problem of planetary motion. Its existence was acknowledged by influential scientists such as H. Poincaré, but not much was known about it. In the first half of the 20th century, chaos started to appear whenever nonlinear differential equations were applied to a problem. An explosion of chaos research – and the establishment of chaos as a separate field of study – occurred in the latter half of the century, when the electric computer allowed the simulation of systems that are too tedious to study by hand. Suddenly chaos was everywhere except for the small confine of analytically solvable models.

One famous example of chaos was given by E. N. Lorenz[9], who studied a simplistic weather model consisting of three coupled first-degree differential equations, two of them nonlinear. He noticed that small changes in the initial

[1] When discussing chaos, mathematics can become a hostile force that opposes human reasoning, when it should be a tool that aids it.

parameters of the model, represented by a truncation of decimal values to three decimal places, changed the long-term behavior of the model completely.

Chaotic behavior is not a special case of dynamical behavior – it is the typical case. An undergraduate physicist does not necessarily encounter chaotic dynamics or the word "chaos" in their studies, but this can be considered as a consequence of physicists preferring models that can be solved with a pen and paper, not as a property of nature. Chaos is everywhere in nature, from the motion of planets to the fluctuations of animal populations.

The fundamental mathematical model for expressing evolution in time, chaotic or otherwise, is the *dynamical system*. A gentle introduction to this topic is given, e.g., in Ref 11. A dynamical system consists of a *phase space* that is the collection of all possible states of a system, and a rule that determines how a given state evolves in time. This rule can be in the form of a first-order differential equation (continuous time parameter) or a function that maps a state to the succedent state (discrete time parameter). The rule establishes, for a given initial phase space point $x(0)$, a unique trajectory $x(t)$ that deterministically describes the state of the system at any future time $t$.

An special subclass of dynamical systems is given by classical mechanics. In its Hamiltonian formulation, the state of the system is given by $n$ generalized coordinates $q_i$ and the corresponding generalized momenta $p_i$, creating a $2n$-dimensional phase space. The time evolution rule is given by Hamilton's equations of motion

$$\dot{q}_i = \frac{\partial H}{\partial p_i} \qquad \text{and} \qquad \dot{p}_i = -\frac{\partial H}{\partial q_i},$$

where $H$ is the Hamiltonian function of the system. If the initial coordinates and momenta $(\boldsymbol{q}, \boldsymbol{p})$ are known, the equations of motion define precisely the coordinates and momenta of the system at any future time – although solving the equations analytically or numerically can be difficult. Hamiltonian dynamics has special properties, such as conservation of the phase space volume, but the dynamics can still be chaotic.

In a generic dynamical system, extreme sensitivity to initial conditions occurs when the distance between two phase space points, initially arbitrarily small, grows exponentially in time. That is, for an initial state $x(0)$ and another initial state $y(0)$ arbitrarily close to it, the distance $\Delta(t) := ||x(t) - y(t)||$ grows as $\Delta(t) \approx \exp(\lambda t)\Delta(0)$. The exponent $\lambda$, which sets the rate of the exponential divergence, is known as the *Lyapunov exponent*. It is a measure of the predictability of the system at this particular initial state $x(0)$. Its inverse is the *Lyapunov time*, which expresses the time scale of the chaotic behavior. For some chaotic systems, such as the solar system, the Lyapunov time is large, so that a fundamentally chaotic system can behave in a seemingly orderly fashion for a long time.

It is easy to see that an exponential divergence leads to practical unpredictability. If in the description above $x$ represents the position of a particle, and the initial position can be measured with an accuracy of $\Delta(0) = 1\,\mu\text{m}$, predictions of its position at time $t$ up to an error tolerance of $\Delta(t) = 1\,\text{mm}$ are possible if

$\lambda t \leq \log(\Delta(t)/\Delta(0)) \approx 7$, or up to seven times the Lyapunov time. To double the time span of predictions with the same error tolerance the precision of the initial measurement would need to be increased by a factor of a thousand to 1 nm. In general, multiplying the initial precision only brings a small additive increase in the predictable time. A long-term forecast for time-scales much larger than the Lyapunov time will quickly end up requiring an initial measurement precision that is beyond any conceivable technology.

By the existence or non-existence of exponential divergence the points in a phase space can be classified into chaotic or not chaotic. A system with no chaotic states is said to be *regular* (or integrable), and a system where all states are chaotic is said to be *fully chaotic*. Both of these are exceptional limiting cases of the generic case of a *mixed system*, where both regular and chaotic motion coexist. In some sources, fully chaotic and mixed behavior are also referred to as *hard* and *soft chaos*, respectively. In a mixed system a natural measure of the overall chaoticity is the relative size of the chaotic fraction of the phase space.

It is intuitively understandable that a sufficiently complicated system, such as the weather on planet Earth, can display such unpredictable behavior. With enough moving parts, accurate predictions on the behavior of any system tends to become more difficult. The truth is, however, that even very simple systems can be chaotic. For this property chaos deserves a certain degree of mystification. How can complicated behavior arise from simple rules?

For a dynamical system, there are certain minimal requirements that are required for chaos. In particular, the system needs to be *nonlinear*, as any linear system can be broken into parts that are too simple to exhibit chaos. For this reason the study of chaos is inseparably connected with the study of nonlinear systems. For smooth continuous-time dynamics another constraint is given by the Poincaré–Bendixson theorem[12], which states that for chaos the dimension of the phase space needs to be at least three.

As long as these two conditions, nonlinearity and at least a three-dimensional phase space, are satisfied, chaos can be found in continuous time dynamics. A particularly simplistic example of chaos is the differential equation[13]

$$\dddot{x} + A\ddot{x} + \dot{x} - |x| + 1 = 0.$$

As a dynamical system it has a three-dimensional phase space, each point being a triplet $z = (x, \dot{x}, \ddot{x})$, and the only source of nonlinearity in the time-evolution rule $\dot{z} = (\dot{x}, \ddot{x}, -1 + |x| - \dot{x} - A\ddot{x})$ is the term $|x|$. Nevertheless, for certain ranges of the parameter $A$, the solution of the differential equation is chaotic.

Even simpler chaotic systems can be found if the prerequisites of the Poincaré–Bendixson theorem are broken. In discrete time, even one-dimensional systems can display chaos. One famous example of this is the *logistic map*[14], where an initial state $x_0 \in ]0, 1[$ evolves according to

$$x_{n+1} = r x_n (1 - x_n).$$

When the parameter $r$ increases over a threshold approximately at $r = 3.56995$ the resulting sequence of values $x_n$ is chaotic. Even though being a second-order polynomial, this mapping has enough curious properties to fill a thesis.

For Hamiltonian mechanics with smooth forces the Poincaré–Bendixson theorem states that the number of generalized coordinates needs to be at least two (in which case the phase space has four dimensions). For classical mechanics the minimal models of chaos therefore involve motion in two dimensions.

A common model of Hamiltonian chaos is the *billiard*: a particle moving without friction in a two-dimensional domain and bouncing from its boundaries by specular reflection[2] (see Fig. 1.1). The dynamics of a billiard is particularly simple because it is determined only by the shape of the boundary curve. The billiards can still exhibit chaotic behavior even for a simple boundary shape.

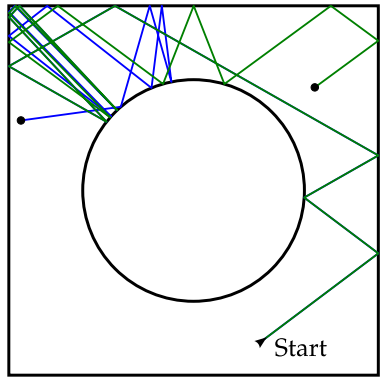


**Figure 1.1.** Chaos in a Sinai billiard. The Sinai billiard[15] consists of a circular scatterer inside a rectangular outer boundary. The lines inside the billiard depict the trajectories of two particles that differ in initial position by five millionths of the square length. After a few reflections this difference is amplified by several orders of magnitude. The final position of the particle depends sensitively on its initial position, i.e., the motion of the particle is chaotic.

Another surprising property of chaos is its *universality*. In many ways, chaos is similar wherever it occurs. An example of such universality is that many systems that become chaotic as a control parameter is changed do so through a cascade of period doublings, which occur at a certain universal rate set by the Feigenbaum constant[16]. For studying chaos this universality is very encouraging. Chaos is not a formless state where no information can be extracted. It can be studied – with simple models, pleasing the reductionist scientist – and this information can be applied to natural phenomena.

[2]Note that the Poincaré–Bendixson theorem does not apply to the discontinuous dynamics given by the reflections, but two dimensions are enough for chaos even with smooth billiard walls.

## 1.2 "There is no quantum chaos"

The first rule of quantum chaos is that there is no quantum chaos. This rule can be derived by applying the concept of a dynamical system to a system governed by quantum mechanics. For the time evolution of a quantum system, the phase space is some Hilbert space $\mathcal{H}$ of state vectors, and the time-evolution of a state vector $|\psi\rangle$ is given by the time-dependent Schrödinger equation (TDSE)

$$\mathrm{i}\frac{\partial}{\partial t}|\psi\rangle = H|\psi\rangle, \tag{1.1}$$

where $H$ is the Hamiltonian operator of the system. The form of Eq. (1.1) already suggests a problem for chaos, as it is a linear equation. Can there be extreme sensitivity to the initial state vector $|\psi(0)\rangle$ in quantum mechanics?

The formal solution of the TDSE for a time-independent Hamiltonian is

$$|\psi(t)\rangle = U(t)|\psi(0)\rangle, \quad \text{with} \quad U(t) = \exp(-\mathrm{i}tH). \tag{1.2}$$

In the above solution, because $H$ is self-adjoint, the time-evolution operator $U$ is unitary. The time-evolution is unitary even if the Hamiltonian is time-independent. The time-evolution operator $U$ only becomes a time-ordered exponential of a continuous family of Hamiltonians at different times.

The unitarity of quantum time-evolution severely limits the sensitivity of a quantum system. Let $|\psi_1(0)\rangle$ and $|\psi_2(0)\rangle$ be two initial quantum states. Their distance at time $t$ is the norm of the vector $|\delta(t)\rangle \coloneqq |\psi_1(t)\rangle - |\psi_2(t)\rangle = U(t)|\delta(0)\rangle$. The squared norm is

$$||\delta(t)||^2 = \langle\delta(t)|\delta(t)\rangle = \langle\delta(0)|\underbrace{U(t)^\dagger U(t)}_{=I}|\delta(0)\rangle = ||\delta(0)||^2.$$

As it should be, a unitary operator $U$ preserves the inner product and thus the norm. Not only does quantum mechanics exclude extreme sensitivity to initial conditions, the distance between two state vectors is *constant* in time.

In the limit of large quantum numbers quantum mechanics needs to reproduce classical results, including chaotic behavior. So how does chaos enter quantum mechanics? This question was the starting point of research initiated in the 1970s. This research is what is now called *quantum chaos*[3]: the research of quantum systems whose classical counterparts are chaotic.

In general, quantum mechanics suppresses chaos in some way, which is beneficial for applications in the quantum regime. This suppression is evident in phenomena such as dynamical localization[18] and quantum scarring. In dynamical localization the diffusion of a periodically disturbed system is suppressed in quantum mechanics. In quantum scarring, which is introduced in Sec 2.3, wave packets launched along unstable periodic orbits keep following the orbit while a corresponding classical probability density is lost in phase space.

[3] There was some dispute[17] over naming a field after something that is proven not to exist, but the name remained.

Everything derived above for the TDSE applies also to some other systems governed by linear wave equations, such as electromagnetic waves. For this reason quantum chaos is also studied under the blanket term *wave chaos*.

Because the main issue of quantum chaos concerns the correspondence between classical and quantum mechanics, quantum chaos is usually studied in the *semiclassical limit*. This is sometimes denoted as the limit $\hbar \to 0$, which involves some abuse of the mathematical concept of a *limit*[4], as quantum mechanics is not a perturbative extension of classical mechanics[17]. What the semiclassical limit means is that the quantum systems are studied when quantum numbers are large (not infinite) and the correspondence of the two theories starts to develop. There is nothing especially interesting in, e.g., the ground states of chaotic systems.

The problem of chaos was already present in the early days of quantum theory when quantum mechanics was developed by quantizing Hamiltonian mechanics. This was done by separating the motion of a particle into distinct periodic oscillations, represented by the action-angle coordinates, and quantizing the classical action of each of these oscillations. However, not all Hamiltonian systems are separable in this way. This was pointed out by none other than A. Einstein, but the full implications of the problem of reconciling classical and quantum mechanics in the presence of chaos were forgotten for decades[19].

Chapter 2 is largely devoted to introducing the theory of quantum chaos, especially the statistical analysis of energy levels, so more will not be said here. A more thorough introduction to the field of quantum chaos can be found, e.g., in Refs. 20–23.

## 1.3 Physics in two dimensions

Physical space consists of three dimensions. Because of this empirical fact the restriction of the number of dimensions to two, as inscribed on the title of this thesis, calls for a short rationale.

In the context of chaos, restricting the number of dimensions to two is justified by two being enough to find chaos in classical mechanics, as discussed in Sec. 1.1. For studying chaos two dimensions is the natural sweet spot, with the third dimension only bringing more complexity but little new insight.

However, two-dimensional systems are not just a convenient theoretical model. In semiconductor heterostructures electrons can be confined to a two-dimensional system[24]. This allows not only new fundamental physics such as the quantum Hall effect[25] but also very practical applications. In fact, in metal–oxide–semiconductor field-effect transistors (MOSFETs), which are the basic building blocks of modern computers, electrons move along a two-dimensional interface[24]. In the current age of graphene[26] and topological insulators[27] there is hardly any need to defend two-dimensional physics.

[4]This limit is especially hard to consider in equations presented in this thesis, since by the choice of units $\hbar = 1$.

# Chapter 2

# Theoretical background

## 2.1 Spectral statistics as quantum fingerprints of chaos

As explained in Sec. 1.2, there is no hope of finding chaos in the perfect unitary time-evolution of a quantum system, at least not as extreme sensitivity to initial conditions[1]. It is then natural to assume that the quantum fingerprints of chaos can be found in the static, time-independent, properties of the system.

As discovered by early quantum chaos researchers, a mark of chaos can be seen in the sequence of real numbers formed by the eigenvalues of the Hamiltonian, i.e., the energy levels of the system. This was a key discovery that directed much of the active quantum chaos research in the 1980s and 1990s. It is curious how the study of chaos in the quantum realm became quite different than in classical mechanics – in the latter, it involves studying points in a phase space and their time-evolution, and in the former it is the statistical analysis of a sequence of numbers.

The rest of this section is devoted to introducing briefly the statistical analysis of energy spectra in the context of quantum chaos, while the next section describes a method for computing the energy spectrum numerically. A more detailed introduction to the topic can be found in any standard text of quantum chaos[20–23].

The main finding of the statistical analysis of quantum eigenvalues is a curious universality. Once the quantum spectrum is properly *unfolded* to remove its smooth (non-universal) part, the regularity or chaoticity of the classical system seems to describe the quantum statistics in a simple parameter-free way. This happens regardless of whether the energy spectrum comes, e.g., from an atom, a nucleus, or a numerical model system.

Firstly, if the classical counterpart is integrable, the quantum eigenvalues seem to follow Poissonian statistics, i.e., they behave as uncorrelated random variables[29]. There are notable counterexamples to this statement, such as the

[1] This should not be understood as a statement that there is nothing scientifically interesting in the time-evolution of quantum systems whose classical counterparts are chaotic. This is proven false by phenomena such as dynamical localization[18,28].

harmonic oscillator, so it should be understood to refer to the typical integrable system.

Similarly, if the corresponding classical system is completely chaotic, the eigenvalues seem to follow statistical distributions derived from random matrix theory (RMT) – the statistical theory of eigenvalues of matrices with random elements[30]. Most notably, spectra of systems with time-reversal symmetry follow the Gaussian orthogonal ensemble (GOE) spectrum, while the Gaussian unitary ensemble (GUE) applies in the absence of time-reversal symmetry. In the presence of spin-orbit interactions, the Gaussian symplectic ensemble (GSE) applies. This characterization of regular and chaotic systems using Poissonian and RMT statistics is known as the Bohigas–Giannoni–Schmit conjecture (BGS)[31]. While originally a conjecture, although supported by a vast array of experimental and numerical evidence, the BGS is also backed by an increasing amount of semiclassical theory[21,32,33].

RMT was originally introduced to physics as a way to model the spectra of complex nuclei[30,32,34]. It was developed substantially in a five-part article by F. J. Dyson and M. L. Mehta[35]. The RMT model was based on a simple working assumption – once the quantum system is complicated enough, with a large number of particles entangled in an intractable web of interactions, the best one can do is to take a Hamiltonian, enforce required symmetry (e.g., time-reversal), and fill the remaining elements with random numbers. This turned out to be a surprisingly successful concept that described well the statistical properties of nuclear spectra[36,37]. What the BGS showed is something even more surprising – that even very simple, but chaotic, systems follow the same statistics.

While the BGS classifies fully chaotic and regular systems very well in terms of their statistical properties, a similar universal description of mixed systems is not known. There are several ways to develop statistics of mixed systems by interpolating between the Poisson and RMT spectra. Examples of such interpolated spectra are the Brody[38] and Berry–Robnik[39] interpolations, latter of which has a better theoretical foundation (for others, see Sec. 3.2.2 in Ref. 21). Fitting such an interpolation on a measured or computed spectrum can be used to extract an interpolation parameter that describes, ideally, how chaotic a system is. Unfortunately the agreement to classical chaoticity measures is often only qualitative, and the interpolation that gives the best agreement is somewhat system-specific. Of course, it is entirely possible – or even likely – that a simple universal theory for mixed systems does not even exist.

Deviations from the universal behavior of RMT can be described in the framework of *periodic orbit theory*. This theory is culminated in the *Gutzwiller trace formula*[40], which expresses the quantum spectrum completely as a sum over periodic orbits of the classical system. Using this formula to actually calculate the quantum spectrum is quite difficult, as the number of periodic orbits in a chaotic system increases exponentially with their length. However, knowledge of even only the shortest periodic orbits provides an accurate description of deviations from the universal limit (see, e.g., Ref. 41). Besides the eigenvalues, the short periodic orbits also have a profound effect to the eigenstates of quantum systems,

as discussed later in Sec. 2.3.

A curious connection, that warrants mentioning whenever spectral statistics are discussed, is that the nontrivial zeros of the Riemann $\zeta$-function (or rather, their imaginary parts) follow GUE statistics with an astonishing precision (see Sec. 8.3.2 in Ref. 21), with corrections given by periodic orbit theory, each prime number representing a periodic orbit[42]. Is there a chaotic quantum system, whose eigenvalues are the imaginary parts of the nontrivial zeros of the Riemann $\zeta$-function? That is, literally, a million dollar question[43].

### 2.1.1 Unfolding the spectrum

Before any universal properties can be inferred from a spectrum of eigenvalues, such as to detect a fingerprint of chaos, the spectrum needs to be *unfolded* to remove the non-universal contributions[23,34]. The details of this process are often omitted in the literature[2]. For example, the monograph by H.-J. Stöckmann ignores the issue completely[21]. However, these details do have an effect on the statistical measures that are used to detect chaos, and subtle mistakes in the unfolding can make a spectrum appear too regular or too chaotic[45–48]. Thus, describing the statistical fluctuations of energy spectra simply as "universal" is somewhat simplifying, as the universal behavior is often revealed only after the non-universal parts have been carefully removed, and subtle ambiguities in this removal process can cause the universal behavior to look very different.

Even before the unfolding, a few preparatory issues need to be addressed. First of all, if the system under study has symmetries (operators that commute with the Hamiltonian), the analysis needs to be carried out for eigenvalues in each symmetry class separately. That is, the entire spectrum must have common good quantum numbers[3]. If different subspectra are mixed together, the total spectrum will appear too regular, because the eigenvalues in different subspectra are uncorrelated. This condition can be difficult to arrange if the symmetries of the system are not fully known.

A similar symmetry-related issue is that non-generic spectra, most notably the harmonic oscillator, can cause misleading results. For example, a separable Hamiltonian constructed from harmonic oscillators and other integrable parts can produce a seemingly "chaotic" spectrum, because the equidistant harmonic oscillator levels produce an imitation of level repulsion[49].

Eigenvalues near the ground state are also discarded, as they are very non-universal. Typically, a few hundred lowest eigenvalues are discarded, depending on how many are available. This causes pressure to develop numerical methods that can compute many eigenvalues of a given system – an issue that we address in Publication II.

Finally, the obtained spectrum needs to be complete, i.e., there must be no missing eigenvalues in the range of the spectrum. The danger of missing (or

[2] For a rare exception, see Ref. 44.

[3] This issue evokes a question – what if there is *near*-symmetry? This question was the starting point of a line of research discussed in Sec. 3.4.

spurious) levels was already pointed out by F. J. Dyson[35d]. This is especially important for experimental studies with a finite resolution, but also for some numerical methods that have difficulties in separating near-degenerate eigenvalues. Missing near-degenerate eigenvalues can cause spectra to look too chaotic, especially if short-range correlations are studied[50].

Even after these conditions are met, there is still plenty of non-universal information in a spectrum of eigenvalues. As a trivial example, an overall energy scale obviously tells nothing about chaoticity. Also, in some systems the density of energy levels increases at higher energies (e.g., a hydrogen atom), for some it decreases (e.g., a particle in a box). This also has no bearing on the issue of chaos. In general, the average, smooth behavior of the density of states is system-specific and not relevant – the universal behavior is seen in the *fluctuations* around this mean behavior.

The unfolding process attempts to produce a spectrum that only contains the fluctuating part of an initial spectrum $E_n$ with $E_0 \leq E_1 \leq E_2 \leq \cdots$. How it is done in practice is best described using the *spectral staircase* function

$$N(E) \coloneqq \#\{E_n \mid E_n \leq E\}. \tag{2.1}$$

As the name suggests, the graph of $N(E)$ is a staircase function, with unit jumps at the eigenvalues $E_n$. If the average behavior of $N(E)$ is known, the spectral staircase can be separated into its average and oscillating part,

$$N(E) = \bar{N}(E) + N_{\text{osc}}(E). \tag{2.2}$$

After this separation is done, the unfolded energy spectrum is defined as

$$\varepsilon_n \coloneqq \bar{N}(E_n). \tag{2.3}$$

This standard exposition of unfolding often leaves the reader somewhat puzzled – and rightfully so. If the purpose of unfolding is to *remove* $\bar{N}$, why the final form *only* depends on $\bar{N}$? For this reason we clarify that, from Eq. (2.2),

$$\bar{N}(E_n) = N(E_n) - N_{\text{osc}}(E_n) = n + 1 - N_{\text{osc}}(E_n). \tag{2.4}$$

That is, the unfolded spectrum (2.3) contains *the fluctuations of the original spectrum, grafted on an artificial background of the sequence of integers*. From this property we also immediately see that the average spacing between values in the unfolded spectrum is one.

The unfolding process is fairly unambiguous if $\bar{N}$ is known accurately from theory. This is the case for, e.g., billiards, where *Weyl's law*[23,51], expresses $\bar{N}$ as a function of the billiard surface area, perimeter, curvature, edges, etc.

If an analytic expression is not known, $\bar{N}$ is estimated from the original spectral staircase. This is when ambiguity creeps into the unfolding process, as the division of an arbitrary curve into a smooth part and an oscillating part is not a mathematically well-defined problem. In the context of statistics, such a division is known as *detrending*.

Traditional ways to extract $\bar{N}$ from $N$ include polynomial fitting, moving averages and low-pass filters. The common weakness in all these methods is that they include an arbitrary external parameter that sets a frequency threshold (or equivalently, a correlation range threshold) that separates $\bar{N}$ from $N_{\mathrm{osc}}$. If $\bar{N}$ is set to follow $N$ too well (a high degree polynomial fit, a small moving average window, or a high frequency cutoff), parts of $N_{\mathrm{osc}}$ start to leak to $\bar{N}$. Vice versa, if, e.g., the polynomial degree is too small, $N_{\mathrm{osc}}$ will contain parts of $\bar{N}$. The improper separation of $\bar{N}$ and $N_{\mathrm{osc}}$ causes spurious long-range correlations, which quite easily cause misleading results[45]. Where the correct parameter value lies needs to be determined by trial and error, and it can be that no such a correct value exists – for example, a certain degree of a polynomial fit might be too low, and the next one too high.

Recently I. O. Morales et al.[46] have suggested that this weakness can be cured – and the ambiguity of the unfolding process greatly reduced – by learning from advances in statistical theory. In the field of time-series analysis, robust, data-adaptive methods have been developed to extract a trend from a sequence of data[52], most notably the empirical mode decomposition (EMD)[53] and its various offsprings. Here *data-adaptive* means that the detrending is done with as few assumptions of the global behavior of the signal as possible, and using the data itself to separate different frequency scales without cutoff parameters. In addition to EMD, it has been recently proposed that ensembles of spectra can be data-adaptively unfolded using the singular value decomposition (SVD)[54].

**Empirical mode decomposition**

EMD is a data-adaptive statistical method that decomposes a signal into oscillatory components separated by the magnitude of their local frequencies, and a residual non-oscillating trend. As such it is useful for detrending the spectral staircase in the unfolding procedure[46]. This method is also the topic of Publication III, which introduces a fast and extensible implementation of EMD and its most popular derivatives. This publication is discussed in more detail later in Sec. 3.3. A more complete introduction to EMD can also be found in Refs. 53, 55, and 56.

The oscillatory components extracted from a signal by EMD are called intrinsic mode functions (IMFs). In comparison to a Fourier decomposition, the oscillatory components are not necessarily sinusoidal. Instead, a much weaker condition is enforced, namely that an IMF is required to have a meaningful *local* frequency[4].

[4]For the following discussion a rigorous definition of a local frequency is not required, but for completeness we summarize it here. The local frequency of a signal $x(t)$ is defined by its Hilbert transform. Let $x_{\mathrm{a}}(t) \coloneqq x(t) + \mathrm{i}\tilde{x}(t)$, where $\tilde{x}$ is the Hilbert transform of $x$. This is known as the *analytic representation* of $x$. The Hilbert transform is defined by

$$\tilde{x}(t) \coloneqq \frac{1}{\pi} \int_{-\infty}^{\infty} \frac{x(u)}{t-u}\,\mathrm{d}u,$$

where the integral is to be understood as a Cauchy principal value. Expressing $x_{\mathrm{a}}$ in polar form, $x_{\mathrm{a}}(t) = A(t)\exp(\mathrm{i}\theta(t))$, defines the local amplitude $A(t)$ and local phase $\theta(t)$ of the original signal. Subsequently the local frequency of the signal is defined as $\omega(t) \coloneqq \theta'(t)$.

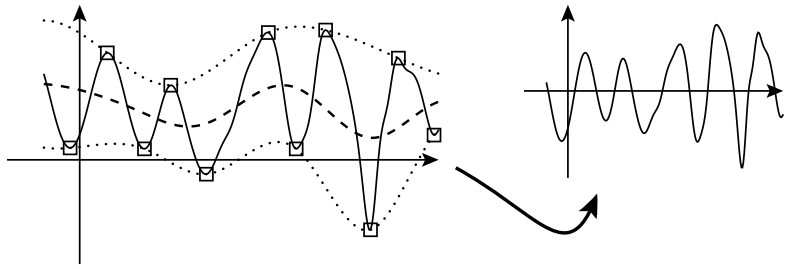

**Figure 2.1.** In the sifting process, an initial signal is separated into a local mean, and the oscillations around the local mean. The original signal (roughly sinusoidal for sake of illustration) is shown in the left panel as a solid line. First, local extrema (open squares) of the signal are located and connected by splines to form the upper and lower envelopes (dotted lines). The mean of these envelopes is designated as the local mean (dashed line). By subtracting the local mean from the original data, a new signal is recovered, as shown in the right panel. This new signal contains the highest frequency oscillations of the original signal in a more symmetric form. The same sifting process is repeated until some stopping criterion is fulfilled, and the result is designated as an IMF.

This is ensured[53] by requiring that for an IMF (1) the number of extrema and the number of zero crossings differ by at most one, and (2) the local mean is zero. In the above definitions (1) is equivalent to requiring that all local maxima of the function are positive and all local minima are negative. These requirements also make an IMF agree with the intuitive picture of what constitutes as "oscillation" around zero.

The IMFs are extracted from the signal in a process known as *sifting*. This proceeds by defining for the signal a local mean, and subtracting the local mean from the original signal to produce a new signal. This new signal, which represents the oscillations around the local mean, is not necessarily symmetric enough to be an IMF, but it is more symmetric than the original one. The sifting process is continued until some stopping criterion is fulfilled, e.g., until the requirements of an IMF are fulfilled, and the number of zero crossings and extrema no longer changes in the process.

In EMD, the local mean of a function is defined by its local extrema. The upper and lower envelopes of a function are formed by connecting the maxima and minima, respectively, with a smooth spline function. The arithmetic mean of these envelopes is then designated as the local mean of the function. This definition and the sifting process are also illustrated in Fig. 2.1. What constitutes as local is therefore not defined by a cutoff parameter, but by the rapidity of the oscillations in the data, adhering to the idea of data-adaptive analysis.

Because of how the local mean is defined, the first IMF extracted from a signal will correspond to the highest frequency oscillations. This IMF is then subtracted from the original data, and the remainder is sifted again to recover the next highest frequency oscillations. This process continues until the remainder is monotonic, at which point the remainder is designated as the trend of the signal.

As seen already from the brief introduction given above, EMD does not completely remove the ambiguity in the detrending process. There are still parameters to be selected, such as the stopping criterion for the sifting and the choice of smooth functions for the envelopes of the signal. However, it is a notable improvement over arbitrarily assuming a low-order polynomial form for the trend, or setting an arbitrary frequency threshold.

Several improved variants of EMD have been developed, most notably ensemble EMD (EEMD)[57] and complete EEMD with adaptive noise (CEEMDAN)[58,59]. Both variants attempt to create a method that more robustly separates components with different frequency scales from the input signal. For example, the methods try to avoid "mode mixing", where two IMFs get suddenly swapped at some point in the time variable due to an accidental local resonance. As such they might not crucially improve the use of EMD for detrending, but as of this writing this has not been studied in the context of energy level statistics. Both of these variants have been implemented in the code described in Publication III.

Both EEMD and CEEMDAN increase the robustness of EMD by employing noise. In EEMD, an ensemble of input signals is created by adding different realizations of small-amplitude white noise to the original signal. After all IMFs have been extracted from each ensemble member, the results are averaged across the ensemble. In the limit of a large ensemble size, the direct effect of the noise is thus removed from the final result. What remains is an indirect smearing effect that helps to remove accidental local effects that can cause, e.g., mode mixing. The downside is that EEMD is no longer a complete decomposition, i.e., the sum of the recovered IMFs and the residual is not exactly equal to the original signal. This is cured in CEEMDAN by performing the averaging over the ensemble for each IMF separately.

### 2.1.2 Statistical measures of quantum chaos

Several statistical measures have been developed to compare observed energy level spectra to predictions given by the BGS. Typically the measures take the form of a univariate probability distribution, so that the comparison can be made simply by comparing graphs in a two-dimensional plot. The traditional statistics introduced briefly in the following section are discussed in more detail in, e.g., Chap. 16 of Ref. 30, which also gives the reference values for the RMT ensembles. In addition to the traditional statistics, we mention some new developments that stem for the association of the fluctuating part of the spectral staircase, $N_{\mathrm{osc}}$, with a time series.

The simplest statistical measure of chaos is the nearest neighbor level spacing (NNLS), i.e., the distribution $P(s)$ of distances $s$ between neighboring energy levels. The NNLS statistic stems from the most easily seen effect of a chaotic spectrum: level repulsion. In chaotic systems the energy levels appear to avoid each other, creating a hole in the NNLS distribution at small $s$. For regular systems the energy levels are uncorrelated, so the NNLS is the exponential distribution $P(s) = \exp(-s)$, which is strongly peaked at small $s$. Thus the NNLS provides an

easy way to differentiate between chaotic and regular behavior, which explains its early success. Its main weakness is that, by definition, it probes only short-range correlations between the energy levels. The unexpected benefit of this weakness is that the NNLS is fairly insensitive to the unfolding process.

Analytic formulas for NNLS distributions for the Gaussian ensembles of RMT are known[30], but quite unwieldy. Typically the NNLS distributions used for comparing results with RMT are approximations, colloquially known as the Wigner surmise[30]. These approximations are

$$P_{\mathrm{GOE}}(s) \approx \frac{\pi}{2} s \exp\left(-\frac{\pi}{4} s^2\right) \tag{2.5}$$

$$P_{\mathrm{GUE}}(s) \approx \frac{32}{\pi^2} s^2 \exp\left(-\frac{4}{\pi} s^2\right), \tag{2.6}$$

i.e., for small spacings $P(s) \approx s$ for GOE and $P(s) \approx s^2$ for GUE. Even though the Wigner surmise is in both cases substantially simpler than the full RMT result, the approximations are very accurate[30,60]. Plots of NNLS distributions for various RMT ensembles can be seen in Fig. 2.2a.

For probing more long-range correlations in the energy spectra, the simplest measure is the *number variance* $\Sigma^2(L)$. Let $n(E, L)$ denote the number of energy levels in an interval of size $L$ at energy $E$. Since the spectrum is unfolded so that the average spacing of energy levels is one, the average of $n$ over all such windows is simply $L$. The number variance is defined to be the variance of $n$, i.e., $\Sigma^2(L) = \langle (n(E, L) - L)^2 \rangle$.

The window size $L$ gives directly the length of the correlations probed by $\Sigma^2$. On the other hand, it can be shown that $\Sigma^2$ only depends on the two-level correlation function (the joint probability distribution of two energy levels), and not on higher order correlations. On the other hand, this makes it easier to calculate RMT predictions for $\Sigma^2$.

For uncorrelated levels $\Sigma^2(L) = L$, and again for RMT spectra somewhat cumbersome analytical formulas exist. At $L \ll 1$, all distributions give almost the same $\Sigma^2(L)$. At large $L$ the RMT results give approximately $\Sigma^2(L) \approx \ln(L)$, so the number variance differs significantly for regular and chaotic systems at large $L$ (see Fig. 2.2b). The intuitive picture is that because of the level repulsion, it is lot less likely that an atypically large amount of levels are packed together in a given interval, so the variance is much smaller.

A historically often-used statistic is the *spectral rigidity* $\Delta_3$, introduced by F. J. Dyson and M. L. Mehta[35d], which is closely related to the number variance. Like $\Sigma^2$, it probes the correlations in an energy interval of size $L$. The definition of $\Delta_3$ is, at first sight, somewhat odd. It is derived by fitting straight lines to the spectral staircase in an energy window of size $L$. As explained in Sec. 2.1.1, the unfolded spectral staircase is a straight line with a unit slope, plus the fluctuations present in the original spectrum. Thus, the discrepancy in a linear fit to the spectral staircase provides a measure on the strength of the fluctuations. With this in

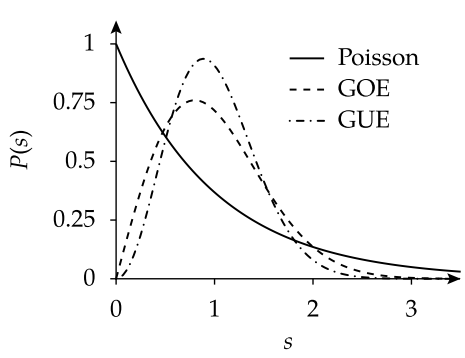


**(a)** NNLS $P(s)$.

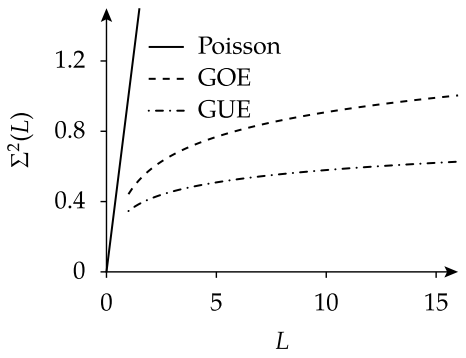


**(b)** Number variance $\Sigma^2$.

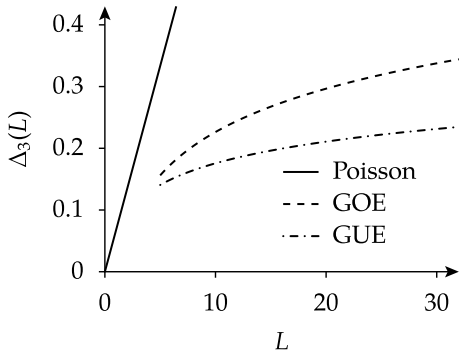


**(c)** Spectral rigidity $\Delta_3$.

**Figure 2.2.** Three traditional eigenvalue statistics, the nearest neighbor level spacing (NNLS), the number variance and the spectral rigidity, evaluated for the cases of uncorrelated energy levels (Poisson statistics), the Gaussian orthogonal ensemble (GOE) and the Gaussian unitary ensemble (GUE). The plot for the NNLS shows the Wigner surmise approximation, and the plots for the number variance and the spectral rigidity use approximate forms valid at large $L$.

mind, the spectral rigidity is defined as

$$\Delta_3(L) = \left\langle \min_{a,b} \int_{E-L/2}^{E+L/2} (N(E) - a - bE)^2 \, \mathrm{d}E \right\rangle, \tag{2.7}$$

i.e., it is the integrated residual of the linear fittings, averaged over all intervals of size $L$.

Similar to the number variance, the spectral rigidity is a linear function of $L$ for regular systems, but grows logarithmically for chaotic systems (see Fig. 2.2c). It can be shown that $\Delta_3$ is essentially a smoothed version of $\Sigma^2$. The spectral rigidity was calculated from semiclassical theory by M. V. Berry using the Gutzwiller trace formula[41] with results that support the BGS. These results also showed

how short periodic orbits cause a saturation of $\Delta_3$ to a finite value at large $L$, where the saturation value depends on the periods of the orbits.

In 2002 A. Relaño et al.[61] proposed that the fluctuating part of the spectral staircase $N_{\text{osc}}$ can be studied directly[5] using methods developed for time-series analysis. In particular, one can study the power spectrum $S(k) \coloneqq |N_{\text{osc}}(k)|^2$, where $N_{\text{osc}}(k)$ is the Fourier transform of $N_{\text{osc}}$. The power spectrum reveals very simple and universal power laws: $S(k) \sim k^{-2}$ for regular systems and $S(k) \sim k^{-1}$ for chaotic systems. These results were also derived from RMT by E. Faleiro et al.[62].

As demonstrated[63] for the Robnik billiard[64], in a mixed system the power spectrum follows a power law $S(k) \sim k^{-\alpha}$, where $\alpha$ changes smoothly from $\alpha = 2$ to $\alpha = 1$ as the system transitions from fully regular to fully chaotic. This makes the power spectrum exponent a very useful measure of chaoticity in mixed systems, especially as $\alpha$ seems to correlate nicely with the classical chaoticity measure, at least for the Robnik billiard. The discovery of a $k^{-1}$ power spectrum in chaotic quantum spectra is also curious on its own right, since the same power spectrum, known as $1/f$ *noise* or "pink noise", is famously ubiquitous in physics (see, e.g. Ref. 65), which can be attributed to *self-organized criticality*[66].

Identifying the oscillations in the spectrum with a time series invites the study of energy level spectra also with other methods commonly used in time series analysis[6]. An example of such a method is detrended fluctuation analysis (DFA)[67] (for an introduction see, e.g., Ref. 68 or Ref. 69). For spectra, DFA is shown to be roughly equivalent to the spectral rigidity[70], except that DFA is somewhat simpler to calculate.

## 2.2 Solving the energy spectrum in real space

Solving the energy spectrum of a quantum system amounts to solving the eigenvalues of the Hamiltonian operator $H$. This problem can be turned into a linear algebra one by expanding $H$ in some countable basis of state vectors $\{\varphi_i\}_i$, and truncating the basis by only including the first $N$ basis vectors. If the truncated basis is sufficiently complete in the sense that the lower energy eigenstates of $H$ are accurately representable as linear combinations of the vectors of the truncated basis, the lower energy eigenvalues of $H$ are very close to the eigenvalues of the $N \times N$ matrix $\boldsymbol{H}$ with elements $H_{ij} = \langle\varphi_i|H|\varphi_j\rangle$. The matrix can be further simplified by, e.g., discarding small elements in order to make the matrix more sparse, or to force the matrix to some kind of special symmetry. Solving the eigenvalues of a matrix is a standard linear algebra problem, for which an entire zoo of different algorithms – which will not be discussed here in detail – has been developed (see, e.g., Ref. 71).

[5] In their original article, A. Relaño et al. study a quantity they call $\delta_n$, which gives the cumulative deviation of the first $n$ level spacings. However, as pointed out by E. Faleiro et al.[62], it can be shown from Eq. (2.4) that this $\delta_n$ is the same as $-N_{\text{osc}}(E_n)$, modulo some constants.

[6] With this idea in mind, it would be interesting to see what information EMD could extract from the spectral staircase, in addition to its trend.

If one wants to use as small matrices as possible, selecting a good basis is essential. Optimizing the basis in this way for each particular problem can be quite time-consuming, especially in systems that lack easy symmetry properties that can be exploited. In the real-space basis, quantum states are represented simply as an array of values of the wave function on a spatial grid. Superficially, the real-space basis is a simple-minded choice that ignores clever system-specific properties. However, the real-space basis is flexible, so that no special symmetry is required of the problem, which can then include, e.g., different length scales, complicated geometries or strong disorder. Thus, a computational method formulated in the real-space basis can be used for a wide range of systems with little preparation. The real-space basis also includes a simple systematic way to improve accuracy by making the grid finer. The downside is that a real-space basis is quite large – for solving the $N$ lowest eigenvalues of a Hamiltonian accurately, the number of grid points needs to be much larger than $N$, typically by a factor of 10 or more.

Luckily, modern eigenvalue solving for large systems uses iterative methods that do not solve all the eigenvalues of a matrix, and do not require that the matrix is stored in memory explicitly. One example of such a *matrix-free* method is the popular Lanczos method[72]. In the Lanczos method, trial vectors are represented in the basis, but the matrix only enters as a routine that computes a product of the matrix with a vector.

In billiard systems the Hamiltonian is simply the Hamiltonian of a free particle, and the only nontrivial dynamics happens at the boundary of the billiard. For these systems special computational methods are available[73]. With these methods extremely high energy states can be solved. However, this section is concerned with the more general (and physically more realistic) case of a smooth, spatially varying potential function.

In this thesis, Sec. 2.2.1 is devoted to introducing imaginary time propagation (ITP), which is a modern iterative method used to solve the $N$ lowest energy eigenstates of a quantum Hamiltonian. The ITP method forms the basis of the numerical program developed in Publication II, and used in Publication IV. In the ITP method, the Hamiltonian is also not expressed in a matrix form, and it only appears in a routine that operates to a trial state vector with $\exp(-\varepsilon H)$, where $\varepsilon > 0$. This operation is handled efficiently with the help of the real-space basis, Fourier transforms, and the separability of the Schrödinger equation. This makes the ITP method a natural real-space method, and a method that is specifically tuned for quantum mechanical Hamiltonians.

When solving the Schrödinger equation numerically for a system of many particles, one quickly hits an exponential wall of computational complexity. This is a result of the vast information content of the many-body quantum state. A particularly clever way to get around this wall is represented by density-functional theory (DFT), introduced later in Sec. 2.2.2. In DFT, the many-body wave function is replaced by the total particle density $n(\boldsymbol{r})$, and the solution of the many-body problem is returned to an effective single-particle problem. This method was used in Publication I to solve the energy spectrum of a many-electron quantum

dot. In DFT, the real-space basis is also a natural choice, as the key quantity is the spatially varying density, and several quantities are naturally expressed as spatial integrals.

### 2.2.1 Imaginary time propagation algorithm

Imaginary time propagation (ITP) is in principle a very general method of solving the lowest eigenvalues and corresponding eigenvectors of any matrix, but its efficient implementation in the context of quantum energy spectra relies on the typical form of single-particle quantum Hamiltonians, and the real-space basis. It was originally described by R. Kosloff and H. Tal-Ezer in 1986[74], based on earlier ideas by M. D. Feit et al.[75].

The basic idea of ITP is simple: for a quantum Hamiltonian $H$ with eigenvalues $E_i$ (with $E_0 \leq E_1 \leq \cdots$) and corresponding orthonormal eigenstates $|\psi_i\rangle$, an arbitrary state $|\varphi\rangle$ can be expanded in basis formed by the eigenstates of $H$ as

$$|\varphi\rangle = \sum_j c_j |\psi_j\rangle,$$

where $\{c_j\}_j$ is some set of (complex) coefficients. Unless the eigenspectrum of $H$ is known (in which case there is no need for ITP) these coefficients are unknown. Nevertheless, operating on the trial state $|\varphi\rangle$ with a cleverly chosen linear operator $\mathcal{T} = \exp(-\varepsilon H)$, with $\varepsilon > 0$, gives

$$\mathcal{T}|\varphi\rangle = \sum_j c_j \mathcal{T}|\psi_j\rangle = \sum_j \Big(c_j \exp(-\varepsilon E_j)\Big)\,|\psi_j\rangle, \tag{2.8}$$

where the last equality follows from $|\psi_j\rangle$ being the eigenstates of $H$.

Whatever the initial coefficients $c_j$ are, it can be seen from Eq. (2.8) that $\mathcal{T}$ causes the coefficients to approach zero[7]. The components with higher energies are diminished exponentially faster than the ones with a lower energy. By repeatedly operating on the same state with $\mathcal{T}$ and normalizing the result, the higher-energy components gradually disappear, leaving only the ground state behind. A similar idea is used in the *inverse iteration* method, in which eigenstates are propagated with an operator that is essentially the inverse of $H$[76].

The procedure of propagating and orthonormalizing can be continued until some desired notion of convergence is achieved. For example, the expectation value of the Hamiltonian $\langle\varphi|H|\varphi\rangle$ can be calculated after each step, and the iteration can be stopped when the value changes only by a negligible amount. Another choice is to follow the decrease of the standard deviation of the Hamiltonian, $\sqrt{\langle\varphi|H^2|\varphi\rangle - \langle\varphi|H|\varphi\rangle^2}$.

The only property that is required from the initial trial state $|\varphi\rangle$ is that it is not orthogonal to any of the wanted eigenstates, i.e., none of the initial coefficients $c_j$ are zero. This condition can be fulfilled with practical certainty by setting the

[7] Assuming $E_0 > 0$, which we can always choose by adding a constant term to $H$.

initial state $|\varphi\rangle$ to random noise. Alternatively, an approximate solution obtained by some other means can be used, if such is available. In practice, a random noise initial state is a perfectly suitable choice due to the exponential speed of the convergence.

In order to recover more eigenstates besides the ground state the same operator $\mathcal{T}$ is applied to each member of a linearly independent ensemble of $N$ initial states. Instead of normalizing each state at each step the whole ensemble is orthonormalized, which preserves the norms of $N$ linearly independent components in the ensemble. Together with the imaginary time propagation, this causes the ensemble to converge towards the $N$ lowest energy eigenstates of $H$.

Another option would be to solve the ground state first, and then project it out from the initial state, obtaining an initial state that converges to the next eigenstate[74]. This can then be repeated to obtain the next eigenstate, and so forth. However, tiny numerical inaccuracies will cause nonzero coefficients for the lowest energy eigenstates to reappear[74], requiring that the projections are applied at each iteration. This quickly becomes infeasible for a large number of eigenstates.

Since the step involving $\mathcal{T}$ is done individually to each trial state it is trivially parallelizable, and in practical computations the orthonormalization step is the computational bottleneck that limits the number of states that can be solved in a given time. It is therefore crucial that the number of iterations (and thus the number of orthonormalizations) is kept minimal. It is also useful to find an orthonormalization algorithm that does not disturb the trial states more than necessary, to not interfere with the convergence.

The name *imaginary time propagation* comes from the operator $\mathcal{T} = \exp(-\varepsilon H)$, which is similar to the standard Schrödinger picture time-evolution operator $U = \exp(-\mathrm{i}tH)$, except for an imaginary value for time, $t = -\varepsilon\mathrm{i}$. For this reason the operator $\mathcal{T}$ is also called the imaginary time propagation operator, and the value $\varepsilon$ the imaginary time step. ITP is also sometimes referred to as the *diffusion algorithm*, due to the way the Schrödinger equation becomes a diffusion equation when transformed to imaginary time.

Publication II deals with the implementation of an efficient eigenvalue solver for two-dimensional single-particle systems. It can routinely solve several thousands of accurate eigenvalues and eigenstates, which can then be used, e.g., to look for fingerprints of quantum chaos. This implementation and its development are described in more detail later in Sec. 3.2.

#### Factorization of the imaginary time propagation operator

The theoretical basis of ITP is simple and easy to state, but a major part of the work required to implement it in practice is hidden in the imaginary time propagation operator $\mathcal{T}(\varepsilon) = \exp(-\varepsilon H)$. This operator cannot be turned into a numerical routine without approximations, and in these approximations the so far arbitrary imaginary time step $\varepsilon$ plays a role.

Unless approximations such as pseudopotentials are involved, the quantum Hamiltonian is of the separable form $H = T + V$. Here operator $T$ is the quantum analogue of the classical kinetic energy, and $V$ includes the external potential and (in a many-particle calculation) possible interactions between particles. This separable form is highly useful because $V$ is diagonal in position space and $T$ is diagonal in $k$-space, and switching between these two spaces is a matter of a simple Fourier transform. Exponentials of both operators $V$ and $T$ are easy to implement, since their exponentials are also diagonal in the same respective bases, and thus they correspond to a simple pointwise multiplication.

To apply ITP in practice we would therefore like to apply the operator $\mathcal{T} = \exp(-\varepsilon(T + V))$ to a quantum state, while we only know how to apply operators $\exp(-\varepsilon T)$ and $\exp(-\varepsilon V)$ separately. This algebraic problem of factorizing exponentials of non-commutative variables is a very general one[77]. It is also encountered, e.g., when the time-propagation operator in Hamiltonian mechanics is factorized to obtain symplectic integrators. The formal solution of the problem is given by the Baker–Campbell–Hausdorff formula (BCH)[78] and the related Zassenhaus formula[78e], which express the exponential $\exp(-\varepsilon(T + V))$ as an infinite product of exponentials of $T$ and $V$ alone. Truncating these formulas can then be used to obtain approximate exponential factorizations that are accurate to some order in the parameter $\varepsilon$.

The simplest nontrivial approximation is a second-order approximation,

$$\begin{aligned} \mathcal{T}(\varepsilon) &= \mathcal{T}_2(\varepsilon) + \mathcal{O}(\varepsilon^3), \\ &\text{with} \quad \mathcal{T}_2(\varepsilon) \coloneqq \exp(-\tfrac{1}{2}\varepsilon V)\exp(-\varepsilon T)\exp(-\tfrac{1}{2}\varepsilon V), \end{aligned} \tag{2.9}$$

which corresponds to the common Verlet integrator in classical dynamics. The approximate ITP operator $\mathcal{T}_2$ is easy to apply to a real-space wave function. The rightmost operator is simply a pointwise multiplication, after which the wave function is Fourier transformed to $k$-space, where the middle operator is $\exp(-\frac{1}{2}\varepsilon k^2)$, i.e., also a multiplication. After Fourier-transforming back to real space the leftmost operator is also a multiplication. In total, each application of $\mathcal{T}_2$ requires three multiplications and two Fourier transforms.

Other approximations for $\mathcal{T}$ similarly involve an error term proportional to some power of $\varepsilon$. Effectively, an approximate $\mathcal{T}$ propagates states towards not the eigenstates of $H$, but towards the eigenstates of an approximate Hamiltonian. Now the imaginary time step $\varepsilon$ is no longer arbitrary. Propagation with a small value for $\varepsilon$ requires several iterations in order for the higher-energy terms to properly vanish, but the results are very accurate. Vice versa, a high value for $\varepsilon$ causes fast convergence, but towards inaccurate results. Practical calculations take this trade-off into account by decreasing the time-step as the calculation progresses. The necessity for approximate propagation operators also creates the need for developing higher-order approximations, in order to use larger time-steps and thus reduce the amount of time-consuming orthonormalization steps.

Arbitrary high order approximations, represented as a product of exponentials,

$$\mathcal{T}(\varepsilon) = \prod_i \exp(c_i \varepsilon V) \exp(d_i \varepsilon T) \tag{2.10}$$

can be derived from the fundamental BCH. The unfortunate side-effect is that the number of terms in the expansion – and thus the amount of computation required for each ITP step – grows exponentially with the order of the expansion. There is another more subtle limitation: in a product expansion of the form (2.10), all the coefficients $c_i$ and $d_i$ need to be negative. Otherwise the particular piece of the propagator propagates the system *backwards* in imaginary time, i.e., the unwanted high-energy terms are explosively *amplified*. Unfortunately, it has been shown that beyond a second-order approximation, such as Eq. (2.9), no higher-order approximation exists with only negative coefficients[79,80].

Several ways to circumvent this problem and derive higher-order propagator approximations have been developed. One possibility is to include in the expansion higher-order commutator terms from the BCH. A particular example is the fourth-order expansion[81]

$$\mathcal{T}_4(\varepsilon) = \exp(-\tfrac{1}{6}\varepsilon V) \exp(-\tfrac{1}{2}\varepsilon T) \exp(-\tfrac{2}{3}\varepsilon W) \exp(-\tfrac{1}{2}\varepsilon T) \exp(-\tfrac{1}{6}\varepsilon V), \tag{2.11}$$

where $W = V + \frac{\varepsilon^2}{48}[V,[T,V]] = V + \frac{\varepsilon^2}{48}|\nabla V|^2$. The new operator $W$ is also diagonal in real space, making this expansion useful in practice. Another option is to generalize the expansion (2.10) to involve complex coefficients (with negative real parts)[82], but this approach already introduces more terms in the fourth order expansion than expansion (2.11)[82b].

A particularly attractive higher-order factorization is possible when the expansion is relaxed from a product to a sum of products. Such a relaxation in the context of classical or quantum real-time propagation would cause the loss of symplecticity or unitarity, respectively, but a similar loss of fundamental mathematical structure does not affect ITP. Such an expansion is derived by S. A. Chin using the second-order expansion (2.9) as a basis and removing error terms with systematic extrapolation[83]. This leads to the arbitrarily high order expansion

$$\mathcal{T}(\varepsilon) = \sum_{k=1}^{n} b_k \mathcal{T}_2^k(\varepsilon/k) + O(\varepsilon^{2n+1}), \tag{2.12}$$

where the coefficients $b_k$ for each $n$ are given by

$$b_i = \prod_{j=1,\ j\neq i}^{n} \frac{i^2}{i^2 - j^2}.$$

In the case of expansion (2.12), the growth of computational complexity as a function of the order is not exponential but quadratic, making it possible to use

very high order approximations in order to reduce the number of time-consuming orthonormalization steps. The quadratic growth is sufficiently modest so that the orthonormalization remains the computational bottleneck, as the propagation part, however complicated for each state individually, is trivially parallelized.

While the expansion (2.12) allows, in principle, arbitrarily high order approximations for $\mathcal{T}$, the applicability of the expansion in practical calculations is limited by finite-precision arithmetic. As the order is increased, at some point the increase in round-off errors from more and more arithmetic operations is larger than the corresponding increase in theoretical accuracy. This saturation order is empirically determined to be approximately 12 for double precision arithmetic[84].

**Including a magnetic field**

Including a magnetic field in the Schrödinger equation amounts to replacing the usual spatial derivative $\boldsymbol{\nabla}$ in the momentum operator by the gauge covariant derivative $\boldsymbol{\nabla} - \mathrm{i}q\boldsymbol{A}$, where $q$ is the charge of the particle, and $\boldsymbol{A}$ is the magnetic vector potential. This is known as *minimal coupling*. For an electron with $q = -1$, this means that the kinetic energy operator becomes $T = \frac{1}{2}\Pi^2$ with a gauge covariant momentum operator $\Pi = -\mathrm{i}\boldsymbol{\nabla} + \boldsymbol{A}$.[8]

The new kinetic energy operator is no longer diagonal in $k$-space, which means further factorization is required to apply $\exp(-\varepsilon T)$ in ITP calculations involving a magnetic field. Luckily, in a uniform magnetic field and with a suitable choice of gauge, the exponential kinetic energy operator can be factorized exactly[85]. Assuming a constant magnetic field $\boldsymbol{B}$ in the $z$-direction and choosing $\boldsymbol{A} = (-By, 0, 0)$,

$$\begin{aligned}\exp(-\varepsilon T) &= \exp\left(-\tfrac{\varepsilon}{2}C_x(\varepsilon B)\Pi_x^2\right)\exp\left(-\tfrac{\varepsilon}{2}C_y(\varepsilon B)\Pi_y^2\right)\exp\left(-\tfrac{\varepsilon}{2}C_x(\varepsilon B)\Pi_x^2\right)\\ &\quad\Big\| \text{ with } C_x(w) = \frac{\tanh(w/2)}{w} \text{ and } C_y(w) = \frac{\sinh w}{w}\\ &= \exp\left(\text{const}\cdot(k_x - By)^2\right)\exp\left(\text{const}\cdot k_y^2\right)\exp\left(\text{const}\cdot(k_x - By)^2\right).\end{aligned} \tag{2.13}$$

The factorized form (2.13) of $\exp(-\varepsilon T)$ can be applied in practice. To operate on a 2D wave function with the rightmost term the wave function is first *partially* Fourier transformed from $(x, y)$ coordinates to $(k_x, y)$. After this transform the rightmost operator is again a simple pointwise multiplication. To apply the middle term, another partial Fourier transform is used to go to $(k_x, k_y)$, and for

[8] With this change the Schrödinger equation acquires the necessary $U(1)$ symmetry of electromagnetism – multiplying wave functions with a phase factor $\exp(\mathrm{i}\Lambda)$ amounts to adding a curl-free term $\boldsymbol{\nabla}\Lambda$ to $\boldsymbol{A}$ (choosing a gauge), and vice versa, without changing any observable quantities. In the case of a time-dependent $\Lambda$, the potential also acquires an extra term $-\partial_t\Lambda$. In fact, this symmetry is why quantum wave functions even have complex values, i.e., that they have a phase. This means that ordinary quantum mechanics is fundamentally a theory about the electromagnetic interaction alone. This well-guarded secret is rarely uttered aloud in introductory quantum mechanics courses.

the leftmost term a transform back to $(k_x, y)$. After a final transform back to $(x, y)$ the full operator has been applied and the wave function is back in real space. The whole ordeal requires the equivalent of two complete Fourier transforms and three multiplications. The version without a magnetic field requires only one multiplication but the same amount of Fourier transforms, so including a magnetic field only adds a relatively small increase in the computational complexity.

One especially appealing property of ITP and the factorization Eq. (2.13) is that the resulting numerical procedure regains at least some of the gauge symmetry of the theory, even taking into account real-space discretization. For example, the choice of coordinate origin in the definition of $\boldsymbol{A}$ can be freely changed, without affecting the calculation[86]. Most numerical schemes involving magnetic fields do not have this property, requiring elaborate selection of the "correct gauge"[9] for each problem, or even for each wave function (see, e.g., Sec. V in Ref. 87).

The factorization in Eq. (2.13) is also exact, in principle, meaning that there are no limits to the strength of the magnetic field. In practice, extremely high magnetic field values can be used. After a certain point finite precision arithmetic starts to create problems, such as numerical underflow due to extremely large negative numbers appearing in the exponentials.

**Subspace orthonormalization**

In addition to propagating the eigenstates in imaginary time, the ITP procedure requires that the eigenstates are orthonormalized after each propagation. In a calculation with many eigenstates, the orthonormalization step is the most computationally intensive one, especially since it is much harder to parallelize efficiently. There are several algorithms available for orthonormalizing a set of vectors. In Publication II we selected subspace orthonormalization (SO)[88], following the advice of previous ITP implementations[84,89,90].

The SO algorithm is most succinctly expressed in a matrix form. Let the input vectors $\boldsymbol{v}_i$ be the columns of a $m \times n$ matrix $\boldsymbol{V}$. For the orthonormalization to make sense, it is assumed that the input vectors are linearly independent. First, let $\boldsymbol{\Delta} = \boldsymbol{V}^\dagger \boldsymbol{V}$, i.e., the elements of $\boldsymbol{\Delta}$ are $\Delta_{ij} = \langle \boldsymbol{v}_i | \boldsymbol{v}_j \rangle$. The $n \times n$ matrix $\boldsymbol{\Delta}$, known as the *Gramian matrix* of the vectors $\boldsymbol{v}_i$, is Hermitian, and also positive definite because the vectors are linearly independent. Therefore it has a spectral decomposition $\boldsymbol{\Delta} = \boldsymbol{U}\boldsymbol{D}\boldsymbol{U}^\dagger$, with a unitary matrix $\boldsymbol{U}$ and a diagonal matrix $\boldsymbol{D}$ with positive diagonal elements. Finally, let $\boldsymbol{W} = \boldsymbol{V}\boldsymbol{U}\boldsymbol{D}^{-1/2}$, where $\boldsymbol{D}^{-1/2}$ is a diagonal matrix such that $D_{ii}^{-1/2} = (D_{ii})^{-1/2}$. Now the column vectors of $\boldsymbol{W}$ span the same space as the initial vectors $\boldsymbol{v}_i$ because $\boldsymbol{U}\boldsymbol{D}^{-1/2}$ is invertible. The column vectors of $\boldsymbol{W}$ are also orthonormal, which can be checked directly by

[9] A categorically absurd concept from the point of view of what a *gauge* means in the theory.

calculating $\boldsymbol{W}^\dagger\boldsymbol{W}$:

$$\boldsymbol{W}^\dagger\boldsymbol{W} = \left(\boldsymbol{V}\boldsymbol{U}\boldsymbol{D}^{-1/2}\right)^\dagger\left(\boldsymbol{V}\boldsymbol{U}\boldsymbol{D}^{-1/2}\right) = \boldsymbol{D}^{-1/2}\boldsymbol{U}^\dagger\overbrace{\boldsymbol{V}^\dagger\boldsymbol{V}}^{\boldsymbol{\Delta}=\boldsymbol{U}\boldsymbol{D}\boldsymbol{U}^\dagger}\boldsymbol{U}\boldsymbol{D}^{-1/2} = \\ = \boldsymbol{D}^{-1/2}\boldsymbol{D}\boldsymbol{D}^{-1/2} = \boldsymbol{I}$$

Computationally, the SO algorithm requires:

- $n(n+1)/2$ inner products to form the matrix $\boldsymbol{\Delta}$
- The diagonalization of the $n \times n$ matrix $\boldsymbol{\Delta}$
- A matrix product of a $m \times n$ matrix and a $n \times n$ matrix

Highly optimized implementations of all these steps are readily available in standard linear algebra libraries. All steps can also be performed without having to store both $\boldsymbol{V}$ and $\boldsymbol{W}$ in memory at the same time, and many parts of the steps can be parallelized. It might seem odd that in order to diagonalize a matrix (to solve the eigenspectrum of a Hamiltonian) we need to diagonalize a matrix (the matrix $\boldsymbol{\Delta}$). However, these two matrices have very different sizes. For $n$ propagated vectors, each having $m$ elements (i.e., the real-space grid has $m$ points), the full Hamiltonian matrix is $m \times m$. The matrix $\boldsymbol{\Delta}$ is $n \times n$. Typically $m \gg n$, making the diagonalization of $\boldsymbol{\Delta}$ a small task compared to the full problem.

As opposed to commonly used Gram–Schmidt orthonormalization (GS), SO is an egalitarian method in a sense that all vectors are treated in the same level of accuracy. In GS one vector is arbitrarily chosen as a reference, and other vectors are orthonormalized sequentially with respect to already treated vectors. This is convenient for some applications since the first output vectors become ready very early into the algorithm. However, this procedure causes numerical errors to distribute quite unevenly across the output vectors. In a test specific to the ITP algorithm, SO was found to cause faster convergence of eigenstates than GS[89].

SO is closely related to the symmetric or Löwdin orthonormalization (LO), which uses $\boldsymbol{W} = \boldsymbol{V}\boldsymbol{U}\boldsymbol{D}^{-1/2}\boldsymbol{U}^\dagger$. LO has the special property that during the orthonormalization the vectors are changed as little as possible[91]. More specifically, among orthonormalization algorithms where the output vectors $\boldsymbol{w}_i$ are a linear transformation of the input vectors $\boldsymbol{v}_i$, LO minimizes the sum $\sum_i ||\boldsymbol{v}_i - \boldsymbol{w}_i||^2$. This might be useful for ITP as some orthonormalizations are performed at a point when most eigenstates are already almost converged, and it is important that they are not disturbed too much.

### 2.2.2 Density-functional theory: From single to many particles

On a fundamental level, solving the Schrödinger equation for more than one electron is not very different from the single-particle case. One needs to be careful about the correct symmetry properties of the wave function, enforced by the indistinguishability of electrons. This also requires taking into account the spin degree of freedom. Otherwise, it is an eigenvalue equation for a linear operator with a simple form. In a typical case, the full Hamiltonian is separable into $H = T + V + W$, where $T$ is the kinetic energy, $V$ is an external potential, and $W$

is the interaction between particles. In principle, this Hamiltonian could be, for example, plugged into the machinery of ITP, if only the symmetry requirements are taken into account.

A direct approach is however computationally quite intractable, except for the case of only a few electrons. This is due to the massive size of the many-body wave function. For $N$ particles, the wave function $\Psi$ is a function of $N$ spatial coordinates. If the spatial coordinates were to be represented by a grid with $K$ points, the wave function would be a multidimensional array of $K^N$ complex numbers. Taking into account the antisymmetry of the wave function reduces this number somewhat, but nevertheless for many particles there is no way to even store the full real-space many-body wave function on a computer, let alone to do operations on it. Due to this explosive growth of required information, it can be argued that the many-body wave function is not even a legitimate scientific concept for a large amount of particles[92].

Luckily it turns out that most of the information contained in the full wave function is quite redundant, and most quantities can be calculated using much simpler objects only. In DFT, it is shown that instead of the wave function, it is sufficient to work with the particle density $n(\boldsymbol{r})$, which is a real-valued function of a single spatial coordinate only. This simplification from $K^N$ to $K$ is computationally quite remarkable.

The basics of DFT are introduced in the following paragraphs for the case of static, or ground-state DFT. This forms a theoretical background for computations performed for Publication I. Extensions and reformulations of DFT to time-dependent problems[93], magnetic fields etc. exist, but will not be discussed here.

At the core of DFT is a seemingly very abstract notion about the functional relationships between the external potential $V$, the ground-state wave function $|\Psi_0\rangle$ and the ground-state density $n_0$. First of all, each $V$ determines a particular $|\Psi_0\rangle$ that is the solution of the Schrödinger equation for the ground state. This equation may be computationally intractable, but the mathematical relationship still exists. Secondly, each $|\Psi_0\rangle$ obviously determines a particular $n_0$. Pictorially, there are mappings

$$V \mapsto |\Psi_0\rangle \mapsto n_0.$$

What is somewhat surprising, but not particularly difficult to prove, is that each of these mappings is in fact injective. Here two potentials are considered different if they differ by more than a constant. This means that there are mappings

$$n_0 \mapsto |\Psi_0\rangle \mapsto V.$$

This result is known as the Hohenberg–Kohn theorem (HK)[94]. It should be noted that since the mapping from $V$ to $|\Psi_0\rangle$ represents the solution of the Schrödinger equation, there is also an implicit dependence on the form of the interaction. Typically the interaction is simply the two-particle repulsive Coulomb interaction.

Despite its abstract nature, the HK has far-reaching consequences. As the ground-state wave function $|\Psi_0\rangle$ is uniquely determined by the ground-state density, the ground-state expectation value $\langle O\rangle \coloneqq \langle\Psi_0|O|\Psi_0\rangle$ of any operator $O$ is also uniquely determined by the ground-state density. Therefore, there exists a function that maps a given ground-state density (also a function) to the corresponding value of $\langle O\rangle$. There is no longer any need for the complicated many-body wave function!

Mathematically, functions that map functions to values are called *functionals*, giving DFT its name. The values of such functions are denoted in the following with square brackets to remind that the elements mapped by the particular functions are themselves also functions.

In particular, the HK tells that the ground-state energy $E_0$ – a quantity of utmost importance in electronic structure calculations – is a functional of $n_0$:

$$E_0[n_0] \coloneqq \langle\Psi_0[n_0]|H|\Psi_0[n_0]\rangle. \tag{2.14}$$

Moreover (assuming a unique ground state for simplicity), if some other density $n$ (not the true ground-state density) were used in this functional, it would produce a different wave function and a larger expectation value for the energy, since $E_0$ is by definition the lowest energy eigenstate. Therefore, the ground state energy of any many-body system can be found by minimizing the functional (2.14).

However, the HK is something what a mathematician would call an existence proof – it provides no way of actually computing values of the functionals. What follows is that the functional $E_0$ is broken into pieces, subtracting dominating contributions that can be calculated from exact theory and proceeding with approximations.

The first simplification comes from the fact that the role of the external potential $V$ in $E_0$ is quite trivial:

$$V[n] \coloneqq \langle\Psi_0[n]|V|\Psi_0[n]\rangle = \int n(\boldsymbol{r})V(\boldsymbol{r})\,\mathrm{d}\boldsymbol{r}. \tag{2.15}$$

The remaining part of the energy functional, the Hohenberg–Kohn functional, $F_{\mathrm{HK}}[n] \coloneqq \langle\Psi_0[n_0]|T+W|\Psi_0[n_0]\rangle = E_0[n] - V[n]$ does not depend on the external potential, so it is universal for all many-body problems with a particular form of the interaction.

The next term that can be subtracted is the classical part of the interaction, i.e., the electrostatic energy of a classical charge density $n$. This is known as the Hartree term, after D. R. Hartree. Denoting the form of the two-particle interaction by $w(\boldsymbol{r},\boldsymbol{r}')$, this term is

$$E_{\mathrm{H}}[n] \coloneqq \tfrac{1}{2}\int n(\boldsymbol{r})n(\boldsymbol{r}')w(\boldsymbol{r},\boldsymbol{r}')\,\mathrm{d}\boldsymbol{r}\,\mathrm{d}\boldsymbol{r}' \tag{2.16}$$

The last remaining challenge is to approximate the kinetic energy part. This can be done using the Kohn–Sham (KS) formalism[95], which uses the HK to return the many-body problem to an effective problem of non-interacting particles.

Keeping in mind that the mappings in the HK exist separately for every kind of interaction $W$, they exist also for the case $W = 0$. So by the HK, for a given external potential $V$ in the interacting problem there is a unique ground-state density $n_0$, and again by the HK, there is a unique external potential $V_\mathrm{s}[n_0]$ in the *non-interacting problem* that produces exactly the same ground-state density $n_0$. This non-interacting problem is known as the Kohn–Sham system of the interacting system.

Being non-interacting, the Schrödinger equation for the KS system separates to a single-particle equation

$$\left(-\tfrac{1}{2}\nabla^2 + V_\mathrm{s}[n_0]\right)\varphi_i = \varepsilon_i \varphi_i, \tag{2.17}$$

which can be solved numerically for a given $V_\mathrm{s}$ using, e.g., ITP.[10] The full ground-state wave function $\Phi_\mathrm{s}$ of the KS is then a Slater determinant of the single-particle wave functions $\varphi_i$, occupied so that the Pauli exclusion principle is satisfied.

It is important to remember that the single-particle states $\varphi_i$ and energies $\varepsilon_i$ solved from the KS are purely auxiliary quantities, that might not necessarily have any resemblance to corresponding quantities in the interacting problem. In practice there usually is at least a qualitative agreement. By design, the single-particle states do however produce exactly the correct density. Additionally, the KS system provides a useful approximation of the kinetic energy part in the ground-state energy functional. The kinetic energy of the ground state in the KS system is

$$T_\mathrm{s} = \sum_i \int |\nabla \varphi_i|^2 \,\mathrm{d}\boldsymbol{r}. \tag{2.18}$$

This quantity is also a functional of the density, since the density determines the effective potential of the KS system, and thus the wave functions $\varphi_i$.

What remains of the energy functional after the contributions from the external potential, the Hartree term, and the KS kinetic energy have been subtracted is denoted the exchange-correlation energy $E_\mathrm{xc}$:

$$E_\mathrm{xc}[n] \coloneqq E_0[n_0] - V[n] - E_\mathrm{H}[n] - T_\mathrm{s}[n]. \tag{2.19}$$

With DFT, all the complications of a many-body quantum problem are hidden in the functional $E_\mathrm{xc}$. The remaining problem is to find good approximations for $E_\mathrm{xc}$.

What has not been addressed so far is how the KS potential $V_\mathrm{s}$ is calculated. Without going too much into detail, it can be derived from Eq. (2.19) by applying variational calculus. Since the ground-state density $n_0$ is, by definition, a density that minimizes the functional $E_0[n]$, the functional derivative of $E_0[n]$ with respect to $n$ is zero at $n_0$. The functional derivatives of $V[n]$ and $E_\mathrm{H}[n]$ are easily

[10] This shows that advances in solving the single-particle equation are useful for solving the many-body problem as well.

calculated,

$$\frac{\delta V[n]}{\delta n(\boldsymbol{r})} = V(\boldsymbol{r})$$
$$\frac{\delta E_{\mathrm{H}}[n]}{\delta n(\boldsymbol{r})} = \int n(\boldsymbol{r}')w(\boldsymbol{r},\boldsymbol{r}')\,\mathrm{d}\boldsymbol{r}' =: V_{\mathrm{H}}(\boldsymbol{r})$$

The remaining derivative of $T_{\mathrm{s}}[n]$ is more involved, since $T_{\mathrm{s}}$ depends on the density implicitly through the solution of the KS system. The result is, however, very useful:

$$\frac{\delta T_{\mathrm{s}}[n]}{\delta n(\boldsymbol{r})} = -V_{\mathrm{s}}(\boldsymbol{r}).$$

Taking functional derivatives of both sides of Eq. (2.19) therefore gives that at the true ground-state density,

$$V_{\mathrm{s}}(\boldsymbol{r}) = V(\boldsymbol{r}) + V_{\mathrm{H}}(\boldsymbol{r}) + V_{\mathrm{xc}}(\boldsymbol{r}), \tag{2.20}$$

where the functional derivative of $E_{\mathrm{xc}}$ is denoted $V_{\mathrm{xc}}$, the exchange-correlation potential. If a good approximation for $E_{\mathrm{xc}}[n]$ (and thus $V_{\mathrm{xc}}$) is known, Eq. (2.20) gives a practical way to calculate $V_{\mathrm{s}}$. This makes it possible to solve the ground-state density by iterating Eqs. (2.17) and (2.20). That is, an approximate density is used to derive a KS potential from Eq. (2.20), which is then plugged into the single-particle Schrödinger equation (2.20), producing an improved density. This density is then improved further, until a convergence is reached. This so-called Kohn–Sham scheme is how DFT is typically used in computations.

The derivation of better and better approximations for $E_{\mathrm{xc}}$ is a large and active field of research, and it will not be discussed here in detail. The simplest approximation is the local density approximation (LDA). In LDA $E_{\mathrm{xc}}$ is calculated for a homogeneous gas of electrons with constant density $n_{\mathrm{const}}$, and an approximation of the general $E_{\mathrm{xc}}$ functional is given by using the same homogeneous result *locally*, by substituting for $n_{\mathrm{const}}$ the true spatially varying density $n(\boldsymbol{r})$. This approximation can be considered applicable when there are no sudden variations in the density. Even though the homogeneous electron gas is a vast simplification, the derivation of a LDA functional requires some fitting to quantum Monte Carlo results. This has been carried out both in 2D[96] and 3D[97]. In practice, LDA works surprisingly well, taking into account its simplicity[98]. The DFT calculations presented in Publication I were also calculated mostly with LDA.

More complicated approximations of $E_{\mathrm{xc}}$ are built up by, e.g., including, in addition to the local density, dependencies on the local gradients of the density, or on the KS eigenstates. This again requires extensive fitting to accurate results on the homogeneous electron gas, other model systems, or experimental data. The resulting functionals are much more computationally intensive to use compared to LDA, but often also more accurate. Unfortunately, this development does not necessarily lead to systematically better approximations to $E_{\mathrm{xc}}$ in a general sense. Some functionals are best suited for particular types of systems, such

as molecules, and some functionals produce accurate predictions of particular physical quantities. Even DFT cannot completely escape from the fact that the many-body quantum problem is a complicated one.

DFT is an extremely popular formalism for studying many-body quantum systems, especially in condensed matter physics and quantum chemistry. By abstracting away the complicated many-body wave function, DFT allows even complex physical and chemical systems to be studied accurately with available computational resources. This is made even easier by the existence of feature-rich publicly available DFT program packages. Some notion about the popularity of DFT is given by citation counts; the original article by P. Hohenberg and W. Kohn[94] has been cited over 17 000 times and the article by W. Kohn and L. J. Sham[95] over 23 000 times – and neither of these are the most cited articles in the field of DFT. W. Kohn shared the 1998 Nobel Prize in Chemistry for his part in the development of DFT.

## 2.3 Quantum scars

Quantum scarring[99] is a phenomenon where the eigenstates of a chaotic quantum system have enhanced probability density around the paths of unstable *classical* periodic orbits[100]. The *instability* of the periodic orbit is a decisive point that separates quantum scars from a more trivial finding that the probability density is enhanced near stable periodic orbits. The latter can be understood as a purely classical phenomenon[100], whereas in the former quantum interference is important. As such, scarring is both a visual example of quantum-classical correspondence, and simultaneously an example of a (local) quantum suppression of chaos[116b].

A classically chaotic system is also ergodic, and therefore almost all of its trajectories eventually explore evenly the entire accessible phase space. It is therefore natural to assume that the eigenstates of the quantum counterpart would fill the quantum phase space evenly (up to random fluctuations) in the semiclassical limit. Scars are a significant correction to this assumption. Scars can therefore be considered as an eigenstate counterpart of how short periodic orbits provide corrections to the universal RMT eigenvalue statistics.

There are rigorous quantum ergodicity theorems proving that the expectation value of an operator converges in the semiclassical limit to the corresponding microcanonical classical average[101]. However, these theorems do not exclude scarring, as the phase space volume of the scars also gradually vanishes in this limit[99,100].

The strength of the scarring effect is determined mainly by how unstable the periodic orbit is. This is expressed by the dimensionless stability exponent $\chi = \lambda T$, where $\lambda$ is the Lyapunov exponent of the orbit – the rate of exponential divergence of trajectories near the orbit – and $T$ is the period of the orbit. How the scarring strength depends on $\chi$ depends on how the strength is defined, but as a general rule of thumb[20] scarring is significant when $\chi < 2\pi$, and the strength of the

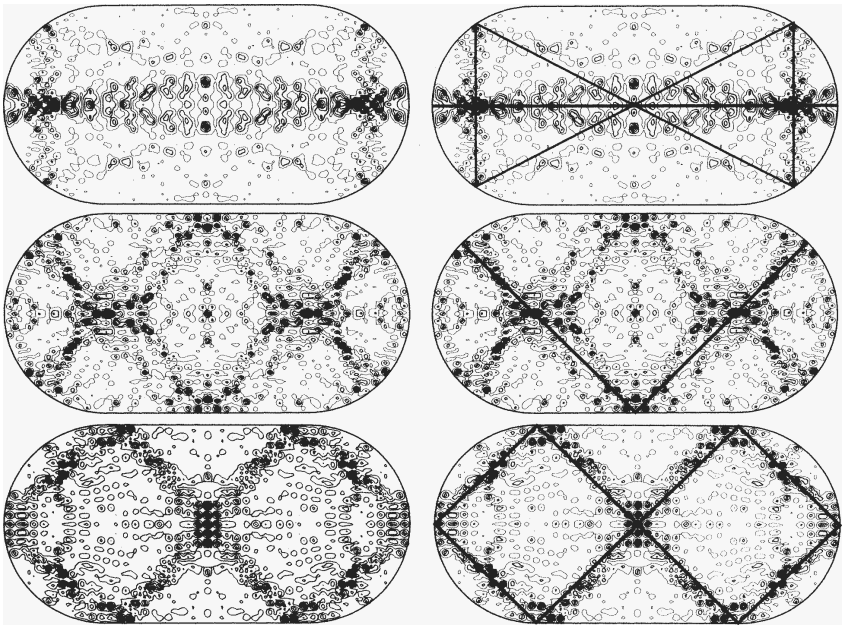

**Figure 2.3.** Examples of scarred eigenstate wave functions (left) with comparisons to the corresponding classical periodic orbits(right) for the stadium billiard. Reprinted figure with permission from: E. J. Heller, "Bound-state eigenfunctions of classically chaotic Hamiltonian systems: scars of periodic orbits", Phys. Rev. Lett. **53**, 1515 (1984)[99]. Copyright 1984 by the American Physical Society.

effect scales as $\chi^{-1}$. Therefore, strongly scarring periodic orbits are unstable, but not too unstable, and relatively short.

First examples of scarred wave functions[11] and a theoretical explanation for their existence were published by E. J. Heller in 1984[99]. The original theory of scarring by E. J. Heller is based on extracting the quantum spectrum by propagating a Gaussian wave packet $|\varphi\rangle$ along the periodic orbit. This theory, which is outlined in the following paragraphs, was later referred to as the linear theory of scarring[104].

In the semiclassical limit, and for a moderately unstable orbit, the Gaussian wave packet remains for short times in a region around the periodic orbit where the dynamics can be linearized. The wave packet will remain centered on the classical orbit for a few periods and only change its shape. In a linear approximation, its width will increase at each iteration by a factor of $\exp(\chi)$ in one direction, and shrink by a factor $\exp(-\chi)$ in the orthogonal direction

[11] What is now known as scarring was described in 1983 by S. W. McDonald in his doctoral thesis on the stadium billiard[102], but only as a potentially interesting numerical observation without a theoretical explanation. It is quite unfortunate for S. W. McDonald and A. N. Kaufman that these findings were not reported in their high-profile article concerning wave functions and NNLS spectra for the stadium billiard[103].

because of phase space volume conservation. The autocorrelation function of the wave packet, $A(t) \coloneqq \langle\varphi|\varphi(t)\rangle$, will show peaks at the multiples of the period $T$, signifying a return of the wave packet to near its initial position. Calculating the overlap of a Gaussian with the same Gaussian stretched by the linearized dynamics gives[100]

$$|A(t = nT)|^2 \approx 1/\cosh(n\chi), \tag{2.21}$$

i.e., the periodic recurrences die out exponentially with a rate set by $\chi$.

The periodic recurrences in $A(t)$ require that the local density of states (LDOS) near the energy of the initial wave packet is strongly peaked. The LDOS near the initial wave packet $|\varphi\rangle$ is defined as

$$S(E) \coloneqq \sum_n |\langle\psi_n|\varphi\rangle|^2 \, \delta(E - E_n),$$

where $|\psi_n\rangle$ and $E_n$ are the eigenstates and corresponding eigenenergies of the system. The Fourier transform of $S(E)$ is $A(t)$:

$$\begin{aligned}\int S(E) \exp(-\mathrm{i}Et) \, \mathrm{d}E &= \sum_n \langle\varphi|\psi_n\rangle\langle\psi_n|\varphi\rangle \exp(-\mathrm{i}E_n t) \\ &= \langle\varphi|\left(\sum_n \langle\psi_n|\varphi\rangle \exp(-\mathrm{i}E_n t)|\psi_n\rangle\right) = \langle\varphi|\varphi(t)\rangle.\end{aligned}$$

If the linearized approximation Eq. (2.21) holds for $A(t)$ at short times, the LDOS, obtained by Fourier transforming the linear approximation, will show[100] a sequence of peaks separated by $2\pi/T$ with widths scaling as $\chi/T$. As shown by E. J. Heller[99], even if the probability amplitude in the LDOS peaks is distributed evenly among the eigenstates near the peak, some of the eigenstates need to have an unusually large overlap with the initial wave packet. As the absolute overlap between an eigenstate $|\psi_n\rangle$ and the wave packet, $|\langle\psi_n|\varphi(t)\rangle|^2$, is time-independent, the eigenstate needs to have a large overlap with the wave packet at all times. Since at least up to $T$ the wave packet follows the path of the classical periodic orbit, the eigenstate needs to have a continuous path of enhanced probability density all along the periodic orbit – a scar.

The linear scarring theory was later extended to include nonlinear effects that occur after the wave packet leaves the linear region around the periodic orbit[104]. These effects can further increase the scarring strength at long times. Alternative theoretical approaches to the wave-packet (or Husimi space) methods employed by E. J. Heller and L. Kaplan include a position-space method by E. B. Bogomolny[105] and a phase-space approach by M. V. Berry[106].

From a computational point of view it is curious that a quantum simulation, even with approximations such as a coarse real-space basis, "senses" the unstable periodic orbits, whereas a classical calculation for locating the orbits requires high numerical accuracy. If simplifying properties such as symmetries are not

available, locating a moderately unstable periodic orbit from a classical system might be simplest to do by solving the time-independent Schrödinger equation!

The first experimental confirmations for scarring were obtained from microwave billiards[107] in 1991. Further experimental results were later obtained for, e.g., quantum wells[108], optical cavities[109] and the hydrogen atom[110]. Recent numerical results also show scars in graphene[111] and atomic gases[112].

There are several phenomena connected – by theory or only by appearance – to quantum scarring. First of all, even random linear combinations of plane waves tend to produce distinct paths of enhanced probability density[113], which needs to be taken into account if scars are to be identified visually. In addition, there are two distinct kinds of scars caused not by actual periodic orbits, but by "ghosts". These ghosts can be periodic orbits that exist in a nearby system, in terms of some external parameter, to the one that is studied[114]. This kind of scarring has also been attributed to almost-periodic orbits[115]. Another type of ghosts come from complex periodic orbits that exist near bifurcations[116].

In Publication IV we extend this list by describing a new kind of scarring, present in symmetric systems disturbed by local perturbations. These scars are not explained by ordinary scar theory. Instead, they are caused by classical resonances in the unperturbed system, as described later in Sec. 3.4.

# Chapter 3

# Main results

This chapter provides a summary of the results presented in the publications included in this thesis. The following sections also provide some more detail – more than the space-constrained articles – on the work that was done to produce the results, and on the background of the research projects. The following sections can therefore be considered as an extra commentary track for the published articles.

## 3.1 Explaining the addition energy spectrum of quantum dashes

The first publication in this thesis[I] represents a step away from the more theoretically oriented world of quantum chaos research. In this work we reproduce numerically the energy spectrum of an actual 2D quantum device, and provide a theoretical explanation for some experimentally observed properties.

The device in question is an indium arsenide (InAs) quantum dash (QDH)[117] – a quantum dot[118] with an elongated shape[1]. Such nanostructures are formed by self-assembly (caused by a lattice mismatch), when InAs is deposited on a suitable crystal surface of a gallium arsenide (GaAs) substrate[120]. The typical size of a QDH is a few hundred nanometers, which is relatively large for a quantum dot. In addition to being elongated along the surface, the QDHs are flat in the vertical direction (approx. 15 nm), making the electronic system inside the device effectively two-dimensional. The typical shape of a QDH as imaged by a scanning electron microscope (SEM) can be seen in Fig. 1b of publication I. In particular the vertical height of the QDHs is also rather asymmetrical.

An experimental group in the University of Tokyo had manufactured the QDH devices and measured their properties. When coupled to electrodes, a QDH operates as a single-electron transistor (SET) – a transistor operating so deep in the quantum regime that the electric current is clearly quantized into

[1] The name dash[119] presumably comes from the device shape, which resembles less a dot (.) and more the neighboring character on the keyboard, a dash (-).

individual electrons. From conductance measurements of a QDH SET and the characteristic Coulomb blockade oscillations, they could deduce the changes in total energy of the dot as it is charged with electrons. For smaller samples they could also resolve the actual number of electrons in the dot, producing a spectrum of *addition energies*[2]

$$\Delta_2(n) = E(n+1) - 2E(n) + E(n-1), \tag{3.1}$$

i.e., the second difference of the $n$-particle ground-state energies $E(n)$.

The experimentalists had observed that the conductance of the device decreases suddenly for electron numbers $n = 7$ and $n = 8$. Their hypothesis was that this is caused by the anisotropic QDH shape. This idea can be explained by a simple particle-in-a-box model. For a rectangular single-particle quantum billiard, some eigenstates will be at the ground state of the longitudinal degree of freedom. If the aspect ratio of the box is high, the probability density in these eigenstates will be very low near the ends of the box. If such a system is connected to a circuit by leads at the ends, the conductance will be low, since an electron in the box is only weakly coupled to the leads.

Our task in the collaboration was to check whether the measured addition energy spectrum could be reproduced by a calculation with interacting electrons in an effective potential. This would show that the observed addition energy spectrum could be explained by the confinement of the electrons to a simple static potential well with a similar asymmetric shape as the QDH. Similar calculations for quantum dots with a more symmetric shape are known to reproduce experimental spectra quite well[118]. We also wanted to see whether the hypothesis for the drop in conductance is supported by a more realistic calculation.

**Experimental setup**

For completeness, we start with a brief review on what the SET setup is, and how the addition energy spectrum was measured from the device. A more complete introduction to SET devices and the Coulomb blockade can be found, e.g., in Ref. 121, Sec. IIB of Ref. 118, and Ref. 122. More details of the sample fabrication and the experimental setup can be found in Publication I.

The classical SET setup (see Fig. 3.1) contains an "island" electrode (in this case, a quantum dot) that is sufficiently decoupled from its environment so that the charge (excess electrons) in the island is clearly quantized in units of the elementary charge. The island is connected to the source and drain electrodes by two tunnel junctions. Electrons can move through the tunnel junctions by quantum tunneling. This process is fast enough that it can be considered instantaneous. A gate electrode is coupled capacitively to the island and is used

[2]In some sources the term *addition energy* is used for $E(n+1) - E(n)$ and $\Delta_2(n)$ in Eq. (3.1) is called the addition energy difference, but a different choice is used here to keep the terminology in line with Publication I. This confusion in the terminology relates to how "energy" is sometimes used to refer to the ground-state energy of the complete $n$-particle system, and sometimes to the energy levels of some effective single-particle system.

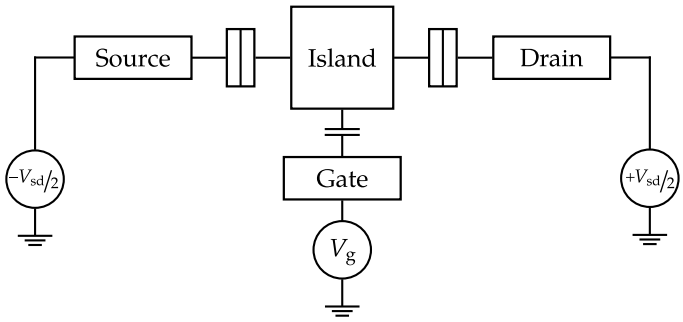


**Figure 3.1.** Schematic circuit diagram of a single-electron transistor (SET). Electrons move by quantum tunneling from the source electrode to the island and from the island to the drain electrode, driven by a bias voltage $V_{sd}$. The electrostatic potential inside the island is controlled by a gate voltage $V_g$, coupled capacitively to the island.

to modulate the electrostatic potential inside the island via a gate voltage $V_g$. In addition, a bias voltage $V_{sd}$ can be applied between the source and drain in order to cause a net flow of electrons through the island.

Due to the quantization of charge inside the island, electrons need to overcome an energy barrier to transfer through the SET. This barrier is the *Coulomb blockade*, and it can be explained with simple classical electrostatics[122]. Assuming that the coupling of the island to its environment can be expressed as a single capacitance $C$, and that the electric potential inside the island is set by the gate voltage $V_g$, the electrostatic energy of the island at charge $q$ is

$$E = qV_g + \frac{q^2}{2C}. \tag{3.2}$$

It is assumed that the bias voltage $V_{sd}$ is just large enough to measure conductance through the system, but tiny enough to be ignored in the electrostatics.

The equilibrium charge $q$ of the island at given $V_g$ is the value that minimizes the energy in Eq. (3.2). The energy as a function of $q$ is a parabola with a minimum at $q_0 = -CV_g$. Due to the quantization of charge, $q$ is restricted to integer multiples of the elementary charge, $q = -ne$. This means that there typically is a nonzero energy barrier that must be overcome to add or remove an electron to the island. In this case – and in this simple approximation – no current flows through the system and the measured conductance is zero.

The Coulomb blockade is lifted when charges $q = -ne$ and $q = -(n+1)e$ have an equal energy. From Eq. (3.2), this occurs when $V_g = (n + 1/2)e/C$. At these specific values, electrons can tunnel in and out of the island with no additional energy barrier, and current flows through the system. If the conductance is measured as a function of $V_g$, this causes periodic peaks separated by $e/C$, with plateaus of near-zero conductance in between. In terms of energy, between successive peaks in conductance where the occupation of the island increases by

a single electron, there is an energy gap of $e^2/C$, which is known as the *charging energy*.

A nonzero bias voltage $V_{\mathrm{sd}}$ helps the electrons overcome the Coulomb blockade. As the bias voltage gives the electrons an additional energy boost proportional to $|V_{\mathrm{sd}}|$, the length of the Coulomb blockade regions in $V_{\mathrm{g}}$ decrease linearly with $|V_{\mathrm{sd}}|$. This means that in a two-dimensional plot where the conductance is measured when both $V_{\mathrm{g}}$ and $V_{\mathrm{sd}}$ are varied – known as a Coulomb stability plot – the regions of Coulomb blockade have a characteristic rhombic shape, known as *Coulomb diamonds*.

The previous, simple theory for the Coulomb blockade is essentially a classical one, only requiring the quantization of charge in the island. As such it can be observed even at relatively high temperatures and large sample sizes, as long as the capacitance $C$ is small enough. When the island becomes very small and the temperature is low enough, the island becomes a true quantum dot with a discrete energy spectrum. This means that for an electron to tunnel into the dot, in addition to the charging energy $e^2/C$ caused by the "classical" Coulomb blockade, it needs energy to cross the gap to the next available energy level of the dot (see, e.g., Ref. 123). This additional energy is called the *orbital (quantization) energy*. Measuring the spacings of the conductance peaks in the Coulomb stability plot and subtracting the charging energy therefore provides a convenient way to measure the single-particle energy spectrum of the quantum dot[124].

The extra energy cost imposed by the discrete level spacing of the dot is $E(n) - E(n-1)$, where $E(n)$ is the ground-state energy of the dot with $n$ electrons. Therefore the spacing between the conductance peaks gives (once the charging energy is subtracted) the second difference of the ground-state energies, i.e. the addition energy in Eq. (3.1). This spectrum of measured addition energies can then be compared with numerical results that use addition energies from numerically calculated values for $E(n)$, obtained, e.g., with ground-state density-functional theory (DFT).

**Numerical calculations**

The first step in the numerical work was to derive a numerical model that could, if possible, reproduce the measured addition energy spectrum. Since the confining potential of the electrons in such an asymmetric quantum dot was not known, we decided to simply start with a semi-realistic parametrization of the potential, deduced from the QDH shape as observed by SEM imaging. In this we decided to aim for simplicity instead of accuracy, as in any case modeling the system as a static potential well is a substantial approximation. For example, the changes in the potential resulting from changes in the gate voltage are ignored in this model. After finding a suitable parametrization of the potential, an optimized potential that reproduced the measured addition energy spectrum as accurately as possible was found by a numerical search algorithm.

The approximate physical size of the QDH sample was measured as 160 nm × 130 nm × 15 nm. As usual, the vertical ($z$-direction) size of the device was small

enough so that the system was assumed to be effectively two-dimensional. The asymmetric height profile of the QDH was assumed to cause an asymmetric confinement potential in the $y$-direction.

As a simple model for the confinement in each direction, we assumed the potential has a power-function form, i.e., $V \sim |2x/L_x|^a$, where $a$ is an adjustable exponent giving the hardness of the confinement and $L_x$ gives a characteristic length-scale. To model the varying hardness of the confinement, other works have used, e.g., a combination of a soft potential and a hard wall[125]. After experimenting with various models we decided to fix the confinement exponent to $a = 2$ in the $y$-direction. Optimized potentials typically settled to a value close to this, and fixing the value helped to reduce the parameter space. A parabolic confinement, i.e., a harmonic oscillator, is a traditional choice for modeling quantum dots[118]. The confinement exponent in the $x$-direction was left as a free parameter to account for effects arising from the source and drain electrodes. The characteristic length scales were set by fixing $L_x$ to the physical size 160 nm and leaving the aspect ratio $r = L_x/L_y$ as a free parameter.

To account for the asymmetric shape in the $y$-direction, the bottom of the parabolic potential well was shifted from the origin by a factor of $\sigma \in [0, 1[$ towards the edge, while keeping the confinement parabolic and keeping potential values at the edge fixed. This was considered as a simple way to model the asymmetry by a single parameter, while keeping the confinement parabolic.

After fixing the overall energy scale by adding an overall multiplicative parameter $V_0$, the functional form of the potential was

$$V(x, y) = V_0 \left( \left( \frac{2y/L_y + \sigma}{1 \pm \sigma} \right)^2 + \left| \frac{2x}{L_x} \right|^a \right), \tag{3.3}$$

where the sign in the term $1 \pm \sigma$ is the sign of $2y/L_y + \sigma$. By fixing $L_x = 160\,\text{nm}$ and $L_y = L_x/r$, the potential is fixed by four parameters, $(V_0, r, a, \sigma)$. We wanted to keep the parameter space relatively small to speed up the optimization process – when the parameters were optimized to reproduce the experimental spectrum, each evaluation of the fitness of a trial potential required the calculation of its ground-state energies for each particle number. A plot of the model potential, with optimized parameters, can be seen in Fig. 3.2.

Calculating the ground-state energy for various particle numbers to get the addition energy spectrum was performed using the DFT formalism introduced in Sec. 2.2.2. An effective-mass approximation was used to take into account the potential of the InAs crystal lattice. Since the ground-state of the system could be spin-polarized (i.e., with nonzero total spin), the calculations were performed in a spin-resolved form. This means that for a given particle number, the calculations were performed for different spin configurations, and the lowest energy configuration was designated as the true ground state.

For approximating the exchange-correlation functional we used the 2D local density approximation (LDA) (or more specifically local spin-density approximation (LSDA), since some calculations involved nonzero total spin). Even though

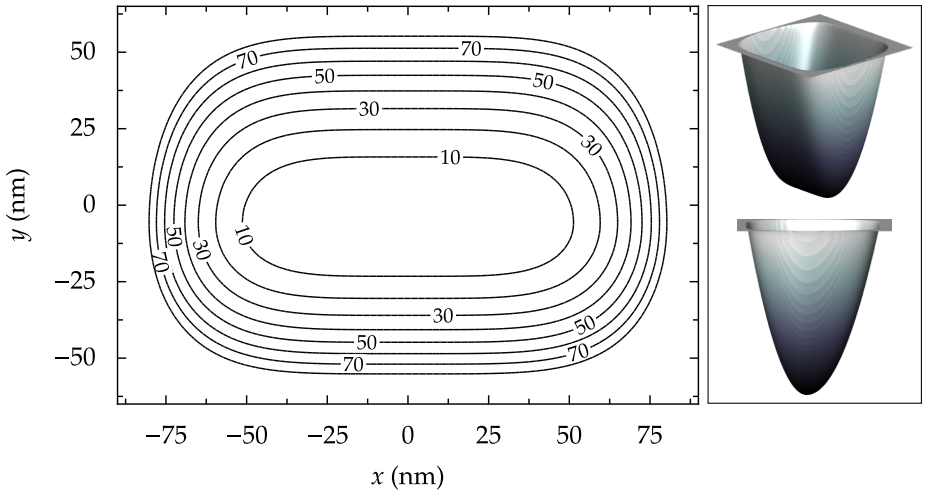


**Figure 3.2.** Contour plot of the optimized asymmetric potential well (3.3) used to model the quantum dash (QDH) confinement in Publication I. Potential values on the contour lines are expressed in meV. The panel on the right shows 3D renderings of the potential shape.

being a relatively simple approximation, it was known to produce accurate results for the addition energy spectra of similar quantum dots[126]. The DFT calculations were performed using the versatile open-source Octopus code package[127].

Ready methods for optimizing the potential to an addition energy spectrum did not exist in Octopus, so the optimizing routine was added in by hand. Due to the lack of a better application programming interface (API), this was done by writing a Python program that provided an interface for programmatic Octopus calculations. The Python program prepared input files for the Octopus program for calculating the ground-state energy of a trial potential for each required $N$ and total spin, waited for the Octopus calculations to finish, and parsed the textual output messages of Octopus to find the ground-state energies. The potential parameters were optimized by minimizing the root mean square (RMS) difference between the experimental and numerical addition energy spectra, weighted by the inverse of experimental error estimates of each data point.

The minimization of the fitness function was performed using the Nelder–Mead downhill simplex algorithm[128], as implemented in the Scipy toolkit[129]. The algorithm locates a minimum of a function in a $d$-dimensional space by moving a simplex (the convex hull of $d + 1$ points) around in the parameter space with a simple heuristic procedure. It is a simple algorithm that rarely provides the fastest or most robust convergence, but for this particular problem it has the advantage that it does not require any knowledge (or approximation) of the derivatives of the fitness function.

**Results**

The numerical search for a suitable potential function did produce a good fit to the experimental addition energy spectrum (see Fig. 3.3), especially considering the uncertainties of the measured values. At the regime of low electron numbers $n \leq 5$ there is substantial discrepancy, which is somewhat understandable as in this regime the effect of the top-gate potential and possible inhomogeneities in the QDH are substantial. In this regime the experimental uncertainties were also very large.

The optimized potential had a slightly asymmetric shape ($\sigma = 0.11$), which suggests that the asymmetric height profile of the QDH really plays a role in the addition energy spectrum. The potential also had a slightly larger aspect ratio ($r = 1.46$) than the exterior of the device ($\tilde{r} = 1.2$), suggesting that the effects of asymmetry (e.g., the lack of a clear shell structure as in a symmetric harmonic potential) are even greater than expected from the device shape alone.

The optimized potential also supported the hypothesis that the decrease of the conductance at $n = 7 \ldots 8$ is related to a sudden change in the shape of the highest occupied single-particle orbital to a form that is more weakly coupled to the leads (see Fig. 4c in Publication I). This comparison was made by studying the highest occupied Kohn–Sham (KS) wave functions. Similar conclusions could be made by studying the difference in the total density[3]. Naturally, estimating the conductance from a static calculation is qualitative at best, and a conclusive proof of the decrease of conductance would require a full quantum transport calculation.

The potential optimization procedure from Publication I was repeated for another sample in a follow-up project[7], which studied the QDHs in high magnetic fields. For this sample the experimental addition energy spectrum was much more accurate. The quality of the sample can also be seen clearly by comparing the Coulomb stability diagram in Fig. 1a of Ref. 7 to Fig. 3a of Publication I.

For the new sample, the asymmetric potential well in Eq. (3.3) did not provide the best fit to the addition energy spectrum. Instead, a simpler symmetric potential well with the confinement exponents as free parameters produced an almost perfect fit (see Fig. 3.4). Naturally this does not rule out asymmetry in the actual confinement, but suggests that its role in the addition energy spectrum is small. In the limit where the asymmetry is small in the area where the electrons are confined, it can become a simple shift of the potential well location, which does not affect the energy spectrum. In the article this difference in the qualitative confinement was attributed to a backgate electrode being used to provide the gating field, whereas Publication I used a top-gate. An inconvenient but possible explanation is that the fit is accidental, especially as in Ref. 7 the parameter space

[3] Assuming a single-particle orbital picture, the difference in the total density when increasing $n$ from 6 to 7 is equal to the squared absolute value of the highest occupied orbital. In this case this difference is very close to the squared absolute value of the corresponding KS wave function. However, the DFT calculation is guaranteed to produce a meaningful total density, whereas the individual KS wave functions are auxiliary quantities that can produce misleading results in some cases.

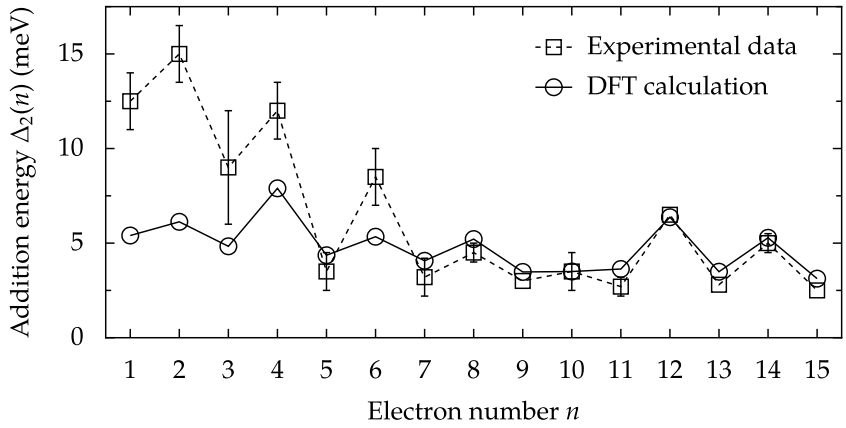


**Figure 3.3.** Comparison of experimental and numerical addition energies from Publication I. The numerical spectrum was calculated with DFT, using LDA and the Octopus code, with a model potential optimized as described in the text. The model potential is also shown in Fig. 3.2. In the experimental spectrum, error bars are not shown for experimental uncertainties below 0.5 meV.

of the potential is five-dimensional.

For Ref. 7 we also attempted to reproduce the experimental results as a function of an external magnetic field. This produced some qualitatively correct features, but not a quantitative match. A better agreement would have required modifying the model to take into account secondary effects from the magnetic field. For example, the effect of the ferromagnetic leads was not taken into account.

### Conclusions

Even though reproducing the addition energy does not prove that the numerical model reflects the true confinement in the QDH device, the numerical results did fulfill their goal and supported the conclusions made from experimental data. The observed addition energy spectrum could be explained by static confinement in a potential well with an asymmetric shape. In addition, the observed decrease in conductance could be attributed to a change in the physical extent of the electronic wave function.

For a theorist, the project also provided a very enlightening view into the world of experimental physics, where the number of unknowns is typically much greater than the number of equations.

In retrospect, the biggest flaw in the potential modeling was that the varying gate potential was not taken into account, i.e., the confinement potential is actually different for each $n$. Substantial improvements could probably be made, especially in the low-$n$ regime, by including these effects even in a simple way.

The method of finding a functional form of the potential by numerical

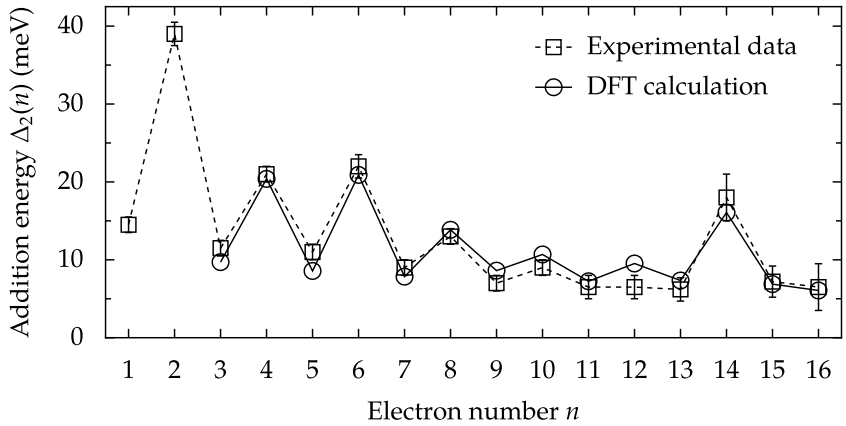


**Figure 3.4.** Comparison of experimental and numerical addition energies, as Fig. 3.3, but for the QDH sample used in Ref. 7. For this sample the experimental uncertainties are much smaller, and the agreement between the experimental and numerical data is also much better. For this case the numerical spectrum for $n < 3$ was not calculated, as the results from Publication I showed that the model fails for very small $n$.

optimization to a measured addition energy spectrum is something that, to our knowledge, has not been performed elsewhere. It would be interesting to try a similar approach to other systems, and see whether it could be used to produce more insight into the actual confinement of electrons inside real devices. Naturally, such studies would need to make sure that the models also have some predictive power, i.e., that the potential obtained by reproducing an addition energy spectrum would also provide quantitatively correct results for some other quantity. After all, a sufficiently complicated model can be fitted to any experimental data.

## 3.2 ITP implementation: `itp2d`

For applying the quantum chaos methodology introduced in Sec. 2.1, we first needed a code that could solve a large number of eigenvalues for various interesting 2D systems. The purpose was to develop a general solver for 2D systems, essentially a piece of code that takes a potential function and produces as many eigenvalues and eigenstates as possible, without, e.g., tailoring basis expansions for each particular problem. We knew imaginary time propagation (ITP) was such a general method, and it could incorporate a strong magnetic field. We also knew that it is suitable for solving a large number of eigenstates.

There were existing ITP codes available, but they were either for 3D systems, or did not include support for a magnetic field. In addition, they were usually designed for a specific purpose, such as solving the Kohn–Sham equations in DFT, and it would have been difficult to modify them for our purposes.

The `itp2d` code was written from scratch using the C++ programming

language. We had previous experience with C++ from writing the `bill2d` code (which was later published[8]). In that project, C++ had proven itself as a useful language to write clearly structured, object-oriented simulation tools, without compromising numerical efficiency. In addition to the C++ core, several data analysis tools and auxiliary tools were written in Python. Python is an interpreted language, making Python code much slower to run, but on the other hand Python is much more modern and flexible. What Python loses in execution time it usually wins, by a landslide, in programming time.

Most of the technical details about the implementation of `itp2d` can be found in Publication II and will not be repeated here. The ITP algorithm was implemented essentially as described in Sec. 2.2.1, using the arbitrarily high order operator factorization (2.12) and using the factorization (2.13) to include a magnetic field. These two recent advances in the ITP method had not been previously implemented in the same publicly available code. State orthonormalization was performed using the subspace orthonormalization (SO) algorithm described in Sec. 2.2.1. The propagation of separate eigenstates and other parts of the algorithms easily amendable to shared-memory parallelization were parallelized using OpenMP[130].

A specific new feature of `itp2d` is the possibility to select Dirichlet boundary conditions instead of the usual periodic ones. This is accomplished by using the discrete sine transform (DST) in place of the usual Fourier transform, as the sine functions are zero at the grid boundary. However, as explained in Publication II, this approach creates a problem. DST still implies periodicity. Even though the values of the wave function at the opposite ends of the grid are the same (i.e., zero), the derivatives are not necessarily the same. This means that when derivatives are computed near the grid boundary with DST, high-frequency ringing artifacts are produced. This is essentially the Gibbs phenomenon. Luckily the artifacts have high frequency, so they are dampened by ITP iterations. However, they still slow convergence, and computing the energy of the eigenstates using the standard deviation of the Hamiltonian becomes inaccurate.

Using the same trick to enforce boundary conditions in the presence of a magnetic field creates further problems, since then the Hamiltonian includes also single derivatives, and therefore sine functions are no longer a good basis. This was taken into account in `itp2d` in a rather *ad hoc* manner by taking care of the cosine terms arising from the single derivatives with the discrete cosine transform (DCT). Again, the resulting Gibbs phenomenon causes slower convergence.

In Sec. 4 of publication II we presented tests on the accuracy of `itp2d` and benchmarks that compare `itp2d` against other publicly available eigensolvers PRIMME[131] and SLEPc[132]. These tests show that `itp2d` can attain a very high accuracy of eigenvalues, and that it is faster than its competitors by a noteworthy margin – although it is unlikely that a single simple benchmark can show this conclusively.

Calculations involving several thousands of eigenstates confirm that the orthonormalization step indeed dominates the computational cost of ITP at this limit. For example, in a calculation with 10 000 eigenstates 97% of the

computational time is spent on performing orthonormalization. If significant performance improvements are required in the limit of many eigenstates, the number of orthonormalization steps needs to be reduced further, and any code optimization should focus on the orthonormalization code.[4]

After completion, `itp2d` became a very useful all-purpose eigenstate solver for following research projects, such as the work on disordered quantum dots that is discussed in Sec. 3.4. In the future, `itp2d` will hopefully find use in the general computational physics community. Besides researchers working on eigenspectrum statistics, there are many fields that would benefit from a fast general-purpose eigenstate solver. One option that has been discussed is the inclusion of `itp2d` as an eigenstate solver for DFT programs such as Octopus[127]. The source code of `itp2d` was published under an open source license and is available at https://bitbucket.org/luukko/itp2d.

There are several ways the ITP method could be developed further. The `itp2d` code is a useful testbed for such development, since it is open source and the different parts of the ITP algorithm are clearly separated in an object-oriented structure. For example, many of the general parameters of the ITP process, such as selection of the imaginary time step $\varepsilon$ and convergence criteria would benefit from a more systematic performance analysis.

As another example, the inclusion of a magnetic field by the exact factorization (2.13) has the displeasing property that the two coefficient functions $C_x$ and $C_y$ are quite unsymmetric[5]. As the magnetic field increases, $C_x$ approaches zero while $C_y$ diverges. The divergence of $C_y$ in the exponential causes problems with finite-precision arithmetic at very large magnetic fields. The factorization was developed in Ref. 85 in a quite indirect manner by noticing an analogy with the density matrix of a harmonic oscillator. This raises the question whether there exists a more symmetric factorization for $\exp(-\varepsilon T)$.

One interesting future prospect would be to use ITP in a basis formed by B-splines instead of a real-space grid. If the exponentiated operator $\exp(-\varepsilon T)$ could be efficiently implemented in this basis, the resulting algorithm would be free from the enforced periodicity and possible Gibbs phenomenon resulting from the use of Fourier transforms.

## 3.3 EMD implementation: `libeemd`

After the `itp2d` project was finished and we had access to energy spectra of a fairly general class of 2D systems, we started to look into energy level statistics with more detail, especially to statistics involving long-range correlations. At this time we learned of the idea by I. O. Morales et al.[46] to use the empirical mode decomposition (EMD) to help with the ambiguity problems inherent in the

[4] In retrospect, many optimizations present in `itp2d` are not terribly useful in the limit of many eigenstates. In fact, `itp2d` could have probably been written entirely in Python since most of the time-consuming calculations are delegated to external linear algebra and fast Fourier transform (FFT) routines. As D. E. Knuth famously put it, *"premature optimization is the root of all evil"*[133].

[5] Note that the factor $C_x$ is shown in a simpler form in (2.13) than in Ref. 85 or Publication II.

unfolding process, and decided to employ EMD for detrending spectral staircases in our analysis. In addition, our research group was already involved with other research involving time series analysis[69,134], where EMD could be highly useful.

There were several existing implementations of EMD. However, these implementations were usually written in Matlab or R, and thus would have been very difficult to incorporate to our existing analysis tools written in Python. In addition, most of the implementations were left in an unfinished state, with outstanding bugs, convoluted code designs and missing documentation. Since EMD is a very active topic of research beyond energy level statistics or even beyond physics, an improved EMD implementation could be very useful for a large audience. This was the beginning of the `libeemd` project.

Several best practices developed in the EMD literature, such as improved stopping criteria and improved EMD variants, were also scattered among different codes. With `libeemd` we wanted to establish a common baseline that collected these improvements to a single code and provided a solid basis for studying and implementing future enhancements.

The `libeemd` library was written using the C programming language, using facilities provided by the GNU Scientific Library (GSL)[135]. C is a usual "lowest common denominator" of programming languages, in the sense that most high-level languages provide ways to call code written in C. Thus writing `libeemd` in C made it easy to write interfaces for calling `libeemd` from other languages.

Using a low-level language also brings a level of speed that is very hard to attain by high-level languages. Although for the purpose of detrending spectral staircases the computational speed is not at all important, for general use speed is often useful. Later benchmarking showed that this difference in speed is quite substantial.

Originally `libeemd` implemented EMD and its most popular variant, ensemble EMD (EEMD). During the reviewing process of Publication III, by request of the anonymous referees, an implementation of a new variant, complete EEMD with adaptive noise (CEEMDAN), was also added. Although `libeemd` was not the first to implement any of these methods, it collected them together and applied several of the best practices discussed in the EMD literature. These included a stopping criterion based on the $S$-number[136] and an extrapolation method for avoiding spurious effects near the ends of the data[57].

Compared to, e.g., the reference EEMD implementation[57], the code also corrected an error regarding the detection of extrema when there are equal consecutive data points in the input signal. Although a numerical corner case, this problem was found to occur in the intermediate steps of EMD with a non-negligible frequency even with random input data.

The processing of separate ensemble members in EEMD and CEEMDAN is trivially parallelized. This was implemented in `libeemd` with OpenMP[130]. As such, `libeemd` provided the first parallel implementation of CEEMDAN.

As an example of a high-level interface for `libeemd`, the library was distributed with a Python interface called `pyeemd`. Python, which we were already very familiar with, provides a standard interface, `ctypes`, to call code written in C.

Together with the numerical facilities provided by the NumPy[137] package, this made it possible to hide the low-level `libeemd` code behind a simple and succinct high-level interface, without losing any of the benefits of a low-level implementation. The `pyeemd` interface was also used to write extensive unit tests to ensure that the underlying code is correct.

By request of the referees of Publication III, an interface to R was also developed. Since neither of the original authors had any experience in R, we delegated the task to J. Helske, who was added as a co-author. Since R is very commonly used in the field of statistics, having a ready R interface will hopefully attract even more users to `libeemd`.

As suspected, by writing the core algorithm in a low-level language such as C, the routines provided by `libeemd` are substantially faster than routines written directly in interpreted languages such as R. In Publication III we benchmarked `libeemd` against two existing R packages[6], `EMD`[138] and `hht`[139]. In these tests `libeemd` was found to be two to three orders of magnitude faster. Even in use cases where EMD is not the bottleneck, this magnitude of improvement is very beneficial.

Although the `libeemd` project grew significantly beyond simply using EMD for unfolding spectra, the implementation will hopefully prove useful far beyond energy level statistics. Hopefully this will justify the scientific detour that was made to create `libeemd`. It is the author's suspicion that EMD and related methods have not nearly reached their full potential, both in the development of the methods, and in the application of the methods to various problems in science.

## 3.4 Strong quantum scars in symmetric systems with local perturbations

Publication IV describes the discovery of a new kind of quantum scarring. This scarring is present in separable systems perturbed by local impurities, and it is not explained by ordinary scar theory as introduced in Sec. 2.3. The road to this discovery was quite long and indirect, so in addition to summarizing the results the steps taken to obtain them are also discussed in the following section.

### Project background

Quantum scarring was not the original topic of the research project. The original goal was to extend the research done in Ref. 140 and study in more detail and in a larger scale how local perturbations (e.g., impurity atoms) affect the energy level statistics of quantum dots. The local perturbations were modeled by

[6] Several existing implementations were written in Matlab. However, as is standard in commercial codes, the Matlab user agreement includes a vague noncompetition clause. This clause seemingly forbids, among other things, benchmarking Matlab against competing products. These kinds of legal shackles are one reason why the author prefers free software.

adding randomly scattered bumps (e.g., Gaussian or Coulombic) to an otherwise separable and classically integrable potential well.

A large number of bumps scattered around in space guarantees that the classical system is, in terms of phase space volume, almost completely chaotic. If the strength of the individual bumps is very low, the Lyapunov time of the system can still be relatively long, placing the system in the realm of *weak chaos*. On the other hand, the quantum spectrum will be close to the unperturbed spectrum if the perturbation is small. For example, for some range in the perturbation strength the spectrum will be accurately described by first-order perturbation theory corrections to the unperturbed spectrum, and it will not be close to a universal random matrix theory (RMT) spectrum.

Since there needs to be a significant discrepancy between the classically chaotic phase space fraction and quantum measures of chaos at small bump strengths, our goal was to study how the correspondence to the RMT spectrum develops as the strength of the impurities is increased, and what is the dependence on the Lyapunov exponent. With `itp2d` this could be studied for a large class of quantum dot potentials and bump shapes, in external magnetic fields, and with different distributions for placing the bumps.

A natural basis for solving the energy spectrum of a perturbed system is the eigenstates of the unperturbed system. However, we decided to use `itp2d` since it was more than capable of solving enough eigenstates for statistical analysis, and trying different systems was quick as there was no need to solve the unperturbed system separately. Even though higher energy eigenstates could be solved by using the unperturbed basis, very high energies are not necessarily very informative as the effect of the finite perturbation vanishes in the limit of very large energies.

The energy level statistics confirmed our expectation that the effect of the original symmetry lingers on for longer than one could expect from the chaoticity of the corresponding classical system, especially in long-range correlations. This also shows that in addition to taking into account symmetries (as discussed in Sec. 2.1.1), *near-symmetries* need to be considered if chaotic properties of a system are inferred by comparing energy level statistics to RMT. These preliminary results, which are unpublished as of this writing, were however eclipsed by what was seen in the eigenstates of the systems.

#### Scar observations

To our surprise, there was extensive and very strong scarring in the eigenstates of the perturbed quantum dot potentials (see Fig. 3.5). This was surprising as random bumps densely covering the potential should eliminate any short periodic orbits. Even if there were some orbits remaining, they should be too unstable to cause scars as strong as seen in the eigenstates. The effect also did not seem to be specific to any particular unperturbed potential or impurity type. Somehow the scarring was caused by the perturbation, as there were no scars in the unperturbed system because of its symmetry. The following research

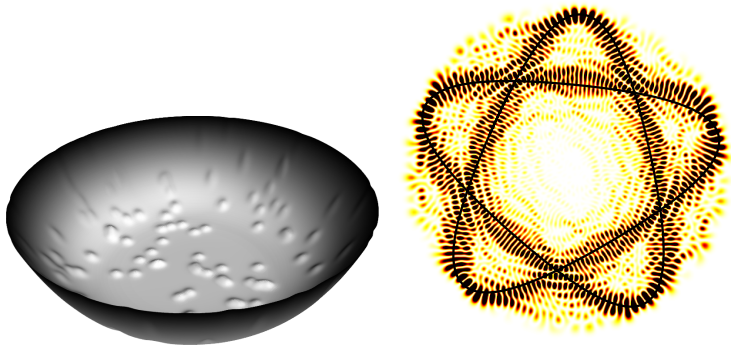

**Figure 3.5.** Example of scarring in perturbed quantum dots. A plot of the potential function is shown on the left. The unperturbed potential is $V(r) = \frac{1}{2}r^5$, and it is perturbed with randomly scattered Gaussian bumps with amplitude $A = 24$. An example of a strongly scarred eigenstate, eigenstate number $n = 2720$, is shown on the right, together with a periodic orbit of the *unperturbed* system for comparison. The energy of the eigenstate is approximately 489, so each individual bump is a small perturbation. There are approximately a hundred bumps in the classically allowed region at this energy.

into what actually is causing the scars was carried out in collaboration with the research group of E. J. Heller and with L. Kaplan.

Of the various unperturbed potentials we had studied so far, the scarring effect appeared to be particularly strong in the case of a circularly symmetric potential well $V(r) \propto r^5$. In this case, the dominant scars looked like rounded five-pointed stars, or pentagrams (see Fig. 3.5), which was soon confirmed to be the shape of the shortest non-trivial periodic orbit of the *unperturbed* potential well. This potential and the pentagram-shaped scars are used in the following discussion as an archetype of perturbation-induced scarring. Since the scarring effect does not appear to be specific to the impurity potential shape, randomly scattered Gaussians with a constant amplitude $A$ and width $w$ are used.

Unperturbed potentials of the form $V(r) \propto r^a$ are especially useful for studying the classical periodic orbits of the unperturbed system. Since the potential function is a homogeneous function of $r$, classical trajectories with any total energy $E$ differ from each other only by a scaling in space and time. Therefore, the shape of periodic orbits does not depend on $E$. Since the potential is also circularly symmetric, its periodic orbits are easily enumerated (see, e.g., Ref. 141 or the supplementary material of Publication IV).

The most natural potential explanation for the scarring was the existence of short, moderately unstable periodic orbits in the perturbed system. This would mean that some periodic orbits of the unperturbed system survive the perturbation, potentially through some nontrivial cancellation of deflections from separate bumps. However, this explanation became unlikely after it was discovered that as a function of the bump amplitude $A$ the scars in each eigenstate did not appear to vanish or even change orientation (see Fig. 3.6). If a scar

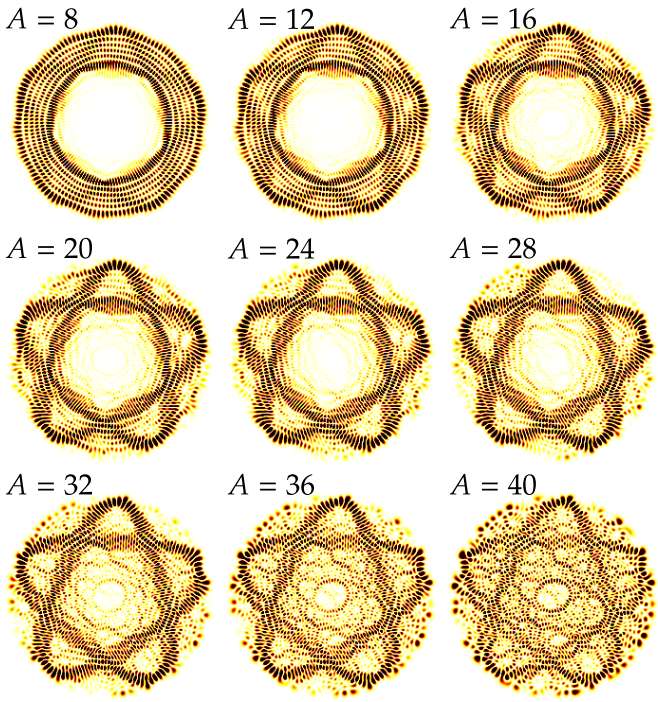


**Figure 3.6.** Scarred eigenstate shown in Fig. 3.5 shown as a function of the impurity amplitude $A$. As $A$ increases the scar becomes more pronounced, until reaching a maximum visibility around $A = 24$ and fading away into a completely delocalized state. During the lifetime of the scar its orientation does not appear to change.

was caused by a "miraculous cancellation" of deflections, the effect should be extremely sensitive to the details of the impurity potential.

The angular orientations of the pentagram-shaped scars also appeared to be fairly constant across a wide range of energies. For a given realization of the random bumps, a few orientations were clearly preferred. This was another proof that the scars were not caused by ordinary scar theory, but instead by some new mechanism[7].

A simple explanation for the preferred orientations would have been that there are gaps in the bumpy potential landscape at certain orientations. Naturally, if an orientation would exist where the pentagram trajectory would not hit any (or would hit atypically few) impurities, it would be much less unstable than the others and thus preferred for scarring. However, this explanation was quickly ruled out by studying systems with only a few bumps. In fact, the opposite of this hypothesis appeared to occur in many cases – the scars often prefer to hit as *many* bumps as possible. This behavior is quite counter-intuitive from the

[7]When discussing names for this apparently new breed of quantum scars the author proposed "quantum scabs", but this was considered too graphic. E. J. Heller used the term "Luukko scars" in his talk given at the 2015 March meeting of the American Physical Society.

point of view of classical stability, and further deepened the mystery of the scars. From an application point of view, the "pinning" of the scars to the impurities is encouraging, since it suggests that the preferred orientations can be selected in a simple way.

**Classical analysis**

To conclusively rule out periodic orbits as the cause of the scars and to find alternative explanations we spent an extensive amount of time studying the classical phase space of the perturbed system. For performing the classical analysis a new C++ code was written. For integrating the classical equations of motion we used the sixth order symplectic integrator by S. Blanes and P. C. Moan[142], which allowed accurate time-propagation even for relatively long times.

Poincaré surface of section plots revealed that there are tiny island structures in the classical phase space for small $A$, but they vanish before the scarring phenomena even reaches its peak as a function of $A$. Moreover, the locations of the last remaining islands did not correspond to the preferred orientations of the scars.

We also investigated *near-periodic* orbits as a possible cause of the scarring. This hypothesis was based on the general tendency of quantum mechanics to smear details of the classical phase space. We also considered the possibility that several near-periodic orbits, located close to each other, could conspire to create the combined recurrence strength to cause scarring. Several near-periodic orbits were found for small values of $A$, but their orientation did not appear to coincide with the orientations of the scars except by accident, and their stability exponents were too large to explain the scarring.

When studying near-periodic orbits in the system we discovered a new method for locating such orbits. This method will be published separately and will not be discussed here in more detail.

**Wave packet analysis**

As described in Sec. 2.3, the recurrence of Gaussian wave packets is a standard tool for studying scars. Because the scars appear in the same preferred orientations across a wide energy range, a single wave packet can localize on many scarred eigenstates. Thus we expected that the recurrences would be exceptionally strong.

For preparing the initial wave packets we used position and momentum coordinates that correspond to an exact periodic orbit in the unperturbed system. The energy of the periodic orbit was set to the energy of the studied scarred eigenstate, and its orientation, parametrized by a rotation angle $\alpha$ was matched with the scar. Propagating the wave packets in time was performed by simply expanding them in the eigenstates of the perturbed system, since they were already available.

To exclude tendency to recur simply due to classical effects (e.g., sticky areas in phase space), we compared the wave packet recurrences to those obtained with classical wave packets, i.e. the propagation of the corresponding classical probability distribution. This distribution is given by the Wigner transform of the quantum wave packet $|\varphi\rangle$,

$$W(\boldsymbol{r},\boldsymbol{p};\varphi) \coloneqq \frac{1}{(2\pi)^3}\int \varphi^*(\boldsymbol{r}+\boldsymbol{r}')\varphi(\boldsymbol{r}-\boldsymbol{r}')\exp(2i\boldsymbol{p}\cdot\boldsymbol{r}')\,\mathrm{d}\boldsymbol{r}'. \tag{3.4}$$

For a Gaussian $|\varphi\rangle$ the Wigner distribution is a multivariate normal distribution. The recurrence strength of $W$ was calculated by sampling many classical initial states $(\boldsymbol{r},\boldsymbol{p})$ from the distribution $W$, propagating each in time, computing $A_W(t) = \sum_i W(\boldsymbol{r}_i(t),\boldsymbol{p}_i(t))$, and normalizing so that $A_W(0) = 1$.

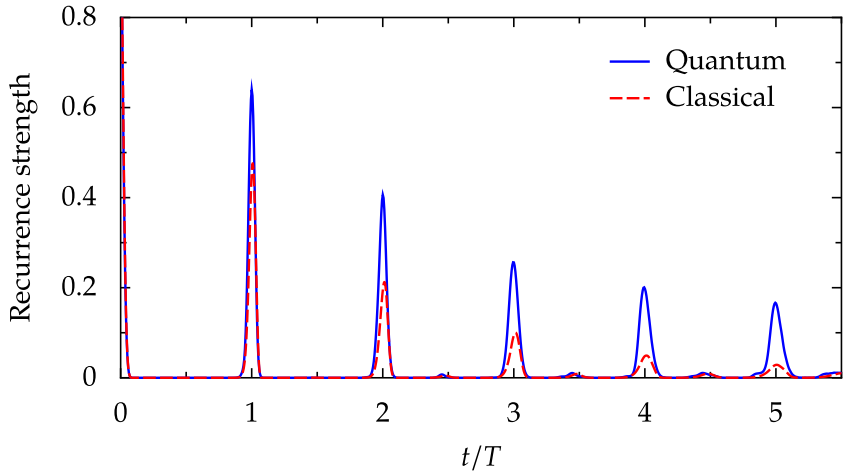


**Figure 3.7.** Recurrence strength $|\langle\varphi|\varphi(t)\rangle|^2$ as a function of time for a Gaussian wave packet $|\varphi\rangle$ running along the scar shown in Fig. 3.5. Clear recurrences are seen with a period that matches with the period $T$ of the unperturbed periodic orbit. Classical recurrences obtained by propagating the corresponding Wigner distribution are substantially weaker.

An example of a resulting recurrence plot can be seen in Fig. 3.7. As suspected, there are clear periodic recurrences, and their period matches with the period $T$ of the unperturbed periodic orbit. The classical recurrences of the corresponding Wigner distribution are much weaker even at short times, showing that the recurrences are not caused by classical stickiness.

To assess the strength of the recurrences it is instructive to compare the heights of the recurrence peaks to the ordinary linear scar theory result in Eq. (2.21). For the recurrences shown in Fig. 3.7 the first recurrence peak is $|A(t=T)|^2 \approx 0.64$, which in linear scar theory would correspond to $\chi \approx 1.0$. For comparison, the least unstable near-periodic orbits found for a smaller bump amplitude $A = 16$ have $\chi \approx 5$. The recurrences, and the scars, are indeed exceptionally strong compared to the stability of the classical system.

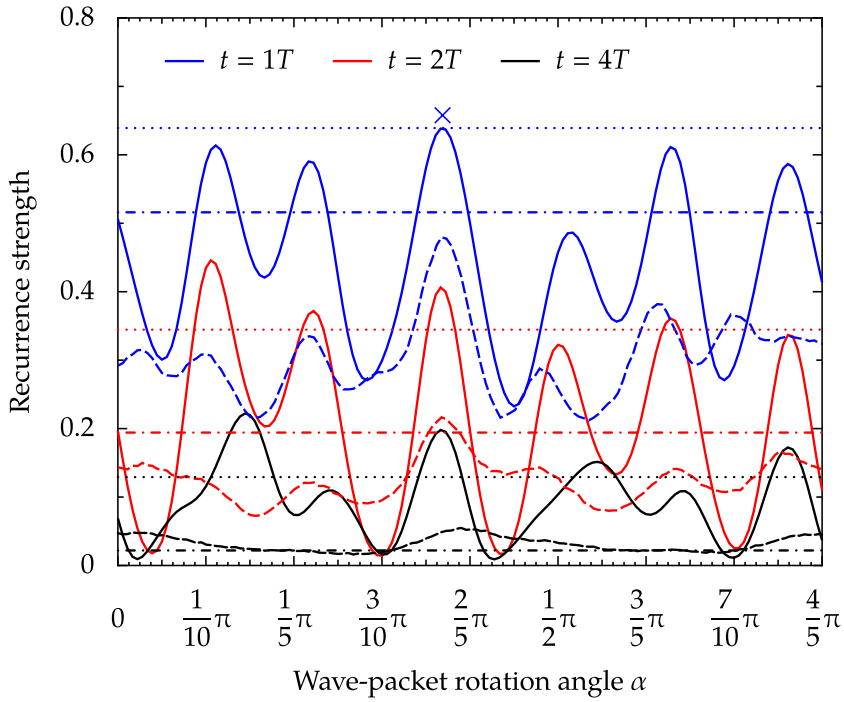


**Figure 3.8.** Heights of the recurrence peaks from Fig. 3.7 shown as a function of the wave packet orientation angle $\alpha$. The value of $\alpha$ used for Fig. 3.7 is marked with a blue cross. The solid lines show the recurrences of the quantum wave packet, and the dashed lines the classical Wigner distributions. Recurrences at $t/T = 1, 2, 4$ are denoted by lines of different colors. In an angular window of $2\pi/5$, after which the pentagram-shaped periodic orbit will be the same, there are three peaks corresponding to the three preferred orientations of scars seen in the particular system. The horizontal lines show the recurrence strengths of the same wave packets without the perturbation, with dash-dotted lines showing the quantum result and dotted lines the classical result.

One particularly interesting result from Publication IV was obtained by looking at how the strengths of the quantum and classical recurrences depend on the orientation angle $\alpha$ of the original wave packet. The resulting plot can be seen in Fig. 3.8. As expected, the preferred orientations of the scars show up as strong peaks at specific values of $\alpha$. What is much less obvious is that the quantum recurrences are stronger than the classical ones even on average, regardless of $\alpha$.

If the recurrence strengths are compared in the unperturbed system (these values are shown as horizontal lines in Fig. 3.8) it can be seen that in that case the classical recurrences are stronger than the quantum ones. Comparing the perturbed and unperturbed recurrences together leads to an even more surprising result – the quantum recurrences in the perturbed system, especially at later times, are stronger than either classical or quantum recurrences in the unperturbed system. It is quite peculiar that adding randomly placed dispersive impurities

can *enhance* the coherent propagation of quantum wave packets. This property of the scars is very promising for possible applications in quantum transport.

**Perturbation theory explanation**

After studying several much more complicated explanations for the scarring seen in the perturbed quantum dot potentials, we found a simple answer in quantum perturbation theory. This explanation, which is described in more detail in Publication IV, is based on two key ingredients. Firstly, there are special near-degeneracies in the eigenstates of the unperturbed system. Thus, a sufficiently small perturbation will form eigenstates that are mostly localized to a subspace spanned by these near-degenerate basis states. Secondly, the localized nature of the perturbation selects scarred states from these subspaces.

The special near-degeneracies mentioned above are connected to classical resonances in the unperturbed system. The classical motion in the unperturbed system is separable to radial and angular oscillations, with oscillation frequencies $\nu_r$ and $\nu_\theta$, respectively. There is a periodic orbit whenever the oscillation frequencies of the two motions are in resonance, i.e., when $\nu_\theta/\nu_r$ is a rational number $a/b$. Similar correspondence of resonances and periodic orbits exists in any separable system.

The energy difference caused by the addition or removal of quanta in the quantum system is approximately proportional to the corresponding classical oscillation frequency. This results from the Bohr–Sommerfeld quantization condition, which is an increasingly accurate approximation in the semiclassical limit of high quantum numbers. Therefore, if a basis state with radial and angular quantum numbers $(r, m)$ is nearby in action to a periodic orbit corresponding to a resonance of the oscillation frequencies $\nu_\theta/\nu_r = a/b$, the state $(r + a, m - b)$ will have approximately the same energy. This requires that both $a$ and $b$ are relatively small integers. Thus shorter periodic orbits correspond to more accurate near-degeneracy, which will lead to stronger scarring.

This classical resonance relation creates a "resonant set" of basis states defined by $(r + ia, m - ib)$ with integer $i$. As the classical oscillation frequencies do not remain constant, all the resonant basis states are not nearly degenerate, but in each resonant set there are some states that are very close to each other in energy.

A sufficiently small perturbation will form eigenstates that are mostly localized to the near-degenerate part of some resonant subspace. Thus these eigenstates of the perturbed system can be approximated by diagonalizing the Hamiltonian in the basis of the nearly-degenerate states[143] – this is nothing but lowest-order perturbation theory in the case of nearly-degenerate states. Since the basis states are almost degenerate, the unperturbed part $H_0$ of the Hamiltonian $H_0 + V_{\text{imp}}$ is approximately only a shift in the eigenvalues, and thus the eigenstates can be approximated further by only diagonalizing the perturbation part of the Hamiltonian $V_{\text{imp}}$ that comes from the impurities.

Because of how the quantum numbers of the resonant states are related to the classical resonances, some linear combinations in the resonant subspace will

trace out the path of the classical periodic orbit. This alone does not explain why such scarred linear combinations are selected by the perturbation.

The scarred linear combinations are preferred because the perturbation $V_{\text{imp}}$ is localized in space into distinct bumps. By the variational principle, when $V_{\text{imp}}$ is diagonalized in the basis of the near-degenerate states, the eigenstate $|\psi\rangle$ that corresponds to the maximal eigenvalue maximizes the expectation value of the perturbation $\langle\psi|V_{\text{imp}}|\psi\rangle$. Similarly the minimal eigenvalue corresponds to minimal $\langle\psi|V_{\text{imp}}|\psi\rangle$. When the perturbation is localized in space, an effective way to extremize this quantity is to form a linear combination that is also localized in space – by selecting a scarred state – and tuning its orientation so that it coincides with as many or as few perturbation bumps as possible. This heuristic argument is substantiated in Publication IV by reproducing the scarred eigenstates by perturbation theory calculations and showing that their orientations extremize $\langle\psi|V_{\text{imp}}|\psi\rangle$.

This theory is very different from the explanation of ordinary scarring, so the two phenomena are connected by appearance but not by cause. The theory explains well the observed properties of the scars that have been described previously, such as the existence of preferred orientations that do not change with $A$, and the observation that scars prefer to pin to the impurities. It also provides an explanation to why the pentagram-shaped scars in the $V(r) \propto r^5$ potential are so strong compared to scars seen in other systems. The pentagram is the simplest star polygon with a self-crossing point. The probability amplitude in a pentagram-shaped scar is concentrated near the self-crossing points, which further strengthens the localization caused by maximizing $\langle\psi|V_{\text{imp}}|\psi\rangle$.

**Possible connections to existing work**

Since the scars are very distinctive and their explanation is fairly simple, we had strong suspicions that we are not the first to come across the phenomenon. However, no clear indication of a previous discovery was found in the literature.

Somewhat similar perturbation-induced scarring has been reported by C. C. Liu et al. in Ref. 144. For a quantum billiard where an originally circular boundary is deformed into a spiral, there are eigenstates with triangle-shaped scars – periodic orbits of the unperturbed circular billiard. However, there is no indication of preferred scar orientations in this case. In addition, it has later been reported, although citing only unpublished data, that such scars are very rare[145].

The scars in the spiral billiard do contain the first ingredient for scars described in Publication IV, namely the near-degeneracy resulting from the symmetry in the circular system. Ref. 144 also discusses the role of degeneracy in the creation of the scarred eigenstates. However, the second ingredient, the local perturbations, is missing. This means that the scarring described in Ref. 144 is related to our work, but substantially weaker.

The interest in the spiral billiard stems from experimental work with spiral-shaped dielectric microcavities[146], which show excellent lasing properties[147]. In these microcavities, resonances in the shape of periodic orbits of the cir-

cular billiard, dubbed *quasiscarred resonances*, are found numerically[148] and experimentally[149].

Even though the existence of short periodic orbits – unstable or otherwise – in the spiral billiard can be easily disproved[148a] (hence the name *quasi*scars), more recent analysis of the quasiscars has revealed that it is not a distinct phenomenon to ordinary scarring. The quasiscarred resonances can be attributed to corrections to ray dynamics that result from the openness of the system[150]. That is, the quasiscarred resonances are *real* scars of a spiral billiard with a modified reflection law, and they are not directly related to scarred eigenstates described in Ref. 144.

Another possibly connected observation is described in Ref. 151, where scarring is studied in a slightly deformed rectangular billiard. Ref. 151 attributes this to ordinary scarring, but it is possible that the scars are linked to the near-degeneracy in the unperturbed system, similarly as in the spiral billiard. The authors of Ref. 151 also do not rule out scarring caused by *stable* periodic orbits.

**Conclusions**

The new type of scarring described in Publication IV is the most important result of this thesis. It is not common to find new physics in the stationary Schrödinger equation. Although connections to existing research was found, the strong scarring caused by symmetries broken by local impurities appears to be overlooked by other researchers. On the other hand, we only found it when not looking for it.

Much of the research on the scarring has so far been concentrated on the prototypical example of the $r^5$ potential. Although instructive for explaining the existence of scars and for presenting initial results, more detailed analysis of the scarring in other systems is required. The theory that explains the scarring is very general, requiring only a separable system and local impurities, so the scarring might prove useful in systems well beyond the simple model systems tried so far.

The wave packet analysis performed for the scars sets the basis of applying the scars in quantum transport, first with more realistic theoretical models and possibly with experiments. From the point of view of applications in transport, Fig. 3.8 summarizes the most interesting property of the scars: recurrences of a wave packet are strengthened – greatly so at late times – in the presence of the impurities. It is a peculiar finding that by adding randomly scattered impurities the transmission of coherent wave packets can be *enhanced*.

Because the preferred orientations of the scars are selected by the impurity positions by scar pinning, the preferred orientations are controllable. Many steps remain between the present study and an application where a local perturbation selectively enhances or suppresses conductance by the manipulation of scarred states, but now the initial step has been taken.

# Chapter 4

# Conclusions and outlook

Concluding notes for each of the publications presented in this thesis were already given in the previous chapter, so the general conclusions left for this chapter will be brief.

The four publications in this thesis – although connected by a background in spectral statistics and quantum chaos in two-dimensional nanostructures – represent four distinct lines of future research.

The first line established that deriving a confinement potential that reproduces a measured addition energy spectrum of a quantum dash can be done with a direct numerical search, thanks to the computational simplicity of density-functional theory (DFT). The models used in Publication I and Ref. 7 are mainly useful for explaining qualitative behavior – as was their purpose – but the same method could be used in a more ambitious setting.

Two of the lines have produced program codes, `itp2d` and `libeemd`, for the solution of common problems, the time-independent Schrödinger equation and the decomposition of data to frequency components and a trend. Although for the purpose of this thesis both Publication II and Publication III were intermediate steps that arose from the need to solve these problems with more flexibility and more efficiency, both projects have future prospects independent of the topic of this thesis. Both codes represent a solid basis for future development of the respective computational methods. Hopefully both `itp2d` and `libeemd` will attract many users (and developers) in the years to come.

As a general remark, the scientific community would benefit from paying more attention to the fostering of high quality, open source program codes, both for the reliability and reproducibility of numerical results, and for avoiding duplicate work.

The final, most vigorous line of future research is the further analysis of the new scars described in Publication IV. Their generality, controllability, and the transport applications hinted by wave packet analysis indicates a bright future for this accidental discovery.

# Glossary

| | |
|---|---|
| 2D | two-dimensional |
| API | application programming interface |
| BCH | Baker–Campbell–Hausdorff formula |
| BGS | Bohigas–Giannoni–Schmit conjecture |
| CEEMDAN | complete EEMD with adaptive noise |
| DCT | discrete cosine transform |
| DFA | detrended fluctuation analysis |
| DFT | density-functional theory |
| DST | discrete sine transform |
| EEMD | ensemble EMD |
| EMD | empirical mode decomposition |
| FFT | fast Fourier transform |
| GaAs | gallium arsenide |
| GOE | Gaussian orthogonal ensemble |
| GS | Gram–Schmidt orthonormalization |
| GSE | Gaussian symplectic ensemble |
| GSL | GNU Scientific Library |
| GUE | Gaussian unitary ensemble |
| HK | Hohenberg–Kohn theorem |
| IMF | intrinsic mode function |
| InAs | indium arsenide |

| | |
|---|---|
| ITP | imaginary time propagation |
| KS | Kohn–Sham, used in terms relating to the Kohn–Sham formalism of DFT |
| LDA | local density approximation |
| LDOS | local density of states |
| LO | Löwdin orthonormalization |
| LSDA | local spin-density approximation |
| MOSFET | metal–oxide–semiconductor field-effect transistor |
| NNLS | nearest neighbor level spacing |
| QDH | quantum dash |
| RMS | root mean square |
| RMT | random matrix theory |
| SEM | scanning electron microscope |
| SET | single-electron transistor |
| SO | subspace orthonormalization |
| SVD | singular value decomposition |
| TDSE | time-dependent Schrödinger equation |

# Bibliography


[I] K. Shibata, K. Seki, P. J. J. Luukko, E. Räsänen, K. M. Cha, I. Horiuchi, and K. Hirakawa, "Electronic structures in single self-assembled InAs quantum dashes detected by nanogap metal electrodes", Appl. Phys. Lett. **99**, 182104 (2011).

[II] P. J. J. Luukko and E. Räsänen, "Imaginary time propagation code for large-scale two-dimensional eigenvalue problems in magnetic fields", Comput. Phys. Commun. **184**, 769 (2013), arXiv:1311.1355 [physics.comp-ph]. Minor correction in: Comput. Phys. Commun. **198**, 262 (2016).

[III] P. J. J. Luukko, J. Helske, and E. Räsänen, "Introducing `libeemd`: a program package for performing the ensemble empirical mode decomposition", Comput. Stat. (2015) 10.1007/s00180-015-0603-9.

[IV] P. J. J. Luukko, B. Drury, A. Klales, L. Kaplan, E. J. Heller, and E. Räsänen, "Strong quantum scarring by random impurities", Phys. Rev. Lett. (2015), arXiv:1511.04198 [quant-ph], submitted.

[5] J. Solanpää, P. J. J. Luukko, and E. Räsänen, "Many-particle dynamics and intershell effects in Wigner molecules", J. Phys.: Condens. Matter **23**, 395602 (2011).

[6] J. Solanpää, J. Nokelainen, P. J. J. Luukko, and E. Räsänen, "Coulomb-interacting billiards in circular cavities", J. Phys. A: Math. Theor. **46**, 235102 (2013), arXiv:1210.2811 [nlin.CD].

[7] K. Shibata, N. Pascher, P. J. J. Luukko, E. Räsänen, S. Schnez, T. Ihn, K. Ensslin, and K. Hirakawa, "Electron magneto-tunneling through single self-assembled InAs quantum dashes", Appl. Phys. Express **7**, 045001 (2014).

[8] J. Solanpää, P. J. J. Luukko, and E. Räsänen, "Bill2d – a software package for classical two-dimensional Hamiltonian systems", Comput. Phys. Commun. **199**, 133 (2016), arXiv:1506.06917 [physics.comp-ph].

[9] E. N. Lorenz, "Deterministic nonperiodic flow", J. Atmos. Sci. **20**, 130 (1963).

[10] B. R. Hunt and E. Ott, "Defining chaos", Chaos **25**, 097618 (2015) 10.1063/1.4922973.

[11] S. H. Strogatz, *Nonlinear dynamics and chaos, With applications to physics, biology, chemistry and engineering*, first paperback printing (Perseus Books Publishing, 1994).

[12] I. Bendixson, "Sur les courbes définies par des équations différentielles", Acta Math. **24**, 1 (1901).

[13] S. J. Linz and J. C. Sprott, "Elementary chaotic flow", Phys. Lett. A **259**, 240 (1999).

[14] R. M. May, "Simple mathematical models with very complicated dynamics", Nature **261**, 459 (1976).

[15] Ya. G. Sinai, "On the foundations of the ergodic hypothesis for a dynamical system of statistical mechanics", Dokl. Acad. Nauk SSSR **153**, (in Russian), 1261 (1963).

[16] M. J. Feigenbaum, "Quantitative universality for a class of nonlinear transformations", J. Stat. Phys. **19**, 25 (1978).

[17] M. Berry, "Quantum chaology, not quantum chaos", Phys. Scripta **40**, 335 (1989).

[18] G. Casati, B. V. Chirikov, F. M. Izraelev, and J. Ford, "Stochastic behavior of a quantum pendulum under a periodic perturbation", in *Stochastic behavior in classical and quantum Hamiltonian systems*, Vol. 93, edited by G. Casati and J. Ford, Lecture Notes in Physics (Springer, 1979), p. 334.

[19] (a) A. Einstein, "Zum Quantensatz von Sommerfeld und Epstein", Verh. Dtsch. Phys. Ges. **19**, 82 (1917); (b) A. D. Stone, "Einstein's unknown insight and the problem of quantizing chaos", Phys. Today **58**, 37 (2005).

[20] M. C. Gutzwiller, *Chaos in classical and quantum mechanics* (Springer, 1990).

[21] H.-J. Stöckmann, *Quantum chaos: an introduction* (Cambridge University Press, New York, 2006).

[22] F. Haake, *Quantum signatures of chaos* (Springer, 2010).

[23] B. Eckhardt, "Quantum mechanics of classically non-integrable systems", Phys. Rep. **163**, 205 (1988).

[24] J. H. Davies, *The physics of low-dimensional semiconductors, An introduction* (Cambridge University Press, 1998).

[25] (a) K. von Klitzing, G. Dorda, and M. Pepper, "New method for high-accuracy determination of the fine-structure constant based on quantized Hall resistance", Phys. Rev. Lett. **45**, 494 (1980); (b) K. von Klitzing, "The quantized Hall effect", Rev. Mod. Phys. **58**, 519 (1986).

[26] (a) K. S. Novoselov, A. K. Geim, S. V. Morozov, D. Jiang, Y. Zhang, S. V. Dubonos, I. V. Grigorieva, and A. A. Firsov, "Electric field effect in atomically thin carbon films", Science **306**, 666 (2004); (b) A. K. Geim and K. S. Novoselov, "The rise of graphene", Nature mat. **6**, 183 (2007); (c) A. K. Geim, "Graphene: status and prospects", Science **324**, 1530 (2009).

[27] M. Z. Hasan and C. L. Kane, "Colloquium: Topological insulators", Rev. Mod. Phys. **82**, 3045 (2010).

[28] F. M. Izrailev, "Simple models of quantum chaos: spectrum and eigenfunctions", Phys. Rep. **196**, 299 (1990).

[29] M. V. Berry and M. Tabor, "Level clustering in the regular spectrum", Proc. R. Soc. Lond. A **356**, 375 (1977).

[30] M. L. Mehta, *Random matrices*, 2nd ed. (Academic Press, 1991).

[31] O. Bohigas, M. J. Giannoni, and C. Schmit, "Characterization of chaotic quantum spectra and universality of level fluctuation laws", Phys. Rev. Lett. **52**, 1 (1984).

[32] T. Guhr, A. Müller-Groeling, and H. A. Weidenmüller, "Random-matrix theories in quantum physics: common concepts", Phys. Rep. **299**, 189 (1998).

[33] S. Heusler, S. Müller, A. Altland, P. Braun, and F. Haake, "Periodic-orbit theory of level correlations", Phys. Rev. Lett. **98**, 044103 (2007).

[34] T. A. Brody, J. Flores, J. B. French, P. A. Mello, A. Pandey, and S. S. M. Wong, "Random-matrix physics: spectrum and strength fluctuations", Rev. Mod. Phys. **53**, 385 (1981).

[35] (a) F. J. Dyson, "Statistical theory of the energy levels of complex systems I", J. Math. Phys. **3**, 140 (1962); (b) "Statistical theory of the energy levels of complex systems II", ibid. **3**, 157 (1962); (c) "Statistical theory of the energy levels of complex systems III", ibid. **3**, 166 (1962); (d) F. J. Dyson and M. L. Mehta, "Statistical theory of the energy levels of complex systems IV", ibid. **4**, 701 (1963); (e) M. L. Mehta and F. J. Dyson, "Statistical theory of the energy levels of complex systems V", ibid. **4**, 713 (1963).

[36] E. P. Wigner, "Random matrices in physics", SIAM Rev. **9**, 1 (1967).

[37] O. Bohigas, R. U. Haq, and A. Pandey, "Fluctuation properties of nuclear energy levels and widths: comparison of theory with experiment", in *Nuclear data for science and technology*, edited by K. H. Böckhoff (Springer Netherlands, 1983), p. 809.

[38] T. A. Brody, "A statistical measure for the repulsion of energy levels", Lett. Nuovo Cimento **7**, 482 (1973).

[39] M. V. Berry and M. Robnik, "Semiclassical level spacings when regular and chaotic orbits coexist", J. Phys. A **17**, 2413 (1984).

[40] M. C. Gutzwiller, "Periodic orbits and classical quantization conditions", J. Math. Phys. **12**, 343 (1971).

[41] M. V. Berry, "Semiclassical theory of spectral rigidity", Proc. R. Soc. Lond. A **400**, 229 (1985).

[42] M. V. Berry, "Semiclassical formula for the number variance of the Riemann zeros", Nonlinearity **1**, 399 (1988).

[43] J. A. Carlson, A. Jaffe, and A. Wiles, eds., *The Millennium Prize problems* (American Mathematical Society, 2006).

[44] H. Bruus and J.-C. Anglès d'Auriac, "Energy level statistics of the two-dimensional Hubbard model at low filling", Phys. Rev. B **55**, 9142 (1997).

[45] J. M. G. Gómez, R. A. Molina, A. Relaño, and J. Retamosa, "Misleading signatures of quantum chaos", Phys. Rev. E **66**, 036209 (2002).

[46] I. O. Morales, E. Landa, P. Stránský, and A. Frank, "Improved unfolding by detrending of statistical fluctuations in quantum spectra", Phys. Rev. E **84**, 016203 (2011).

[47] E. Haller, H. Köppel, and L. S. Cederbaum, "On the statistical behaviour of molecular vibronic energy levels", Chem. Phys. Lett. **101**, 215 (1983).

[48] C. Schlier, "How much can we learn from nearest neighbor distributions?", J. Chem. Phys. **117**, 3098 (2002).

[49] S. Drożdż and J. Speth, "Near-ground-state spectral fluctuations in multi-dimensional separable systems", Phys. Rev. Lett. **67**, 529 (1991).

[50] L. Michaille and J.-P. Pique, "Influence of experimental resolution on the spectral statistics used to show quantum chaos: the case of molecular vibrational chaos", Phys. Rev. Lett. **82**, 2083 (1999).

[51] H. P. Baltes and E. R. Hilf, *Spectra of finite systems* (Bibliographisches Institut, 1976).

[52] Z. Wu, N. E. Huang, S. R. Long, and C.-K. Peng, "On the trend, detrending, and variability of nonlinear and nonstationary time series", Proc. Natl. Acad. Sci. U.S.A. **104**, 14889 (2007).

[53] N. E. Huang, Z. Shen, S. R. Long, M. C. Wu, H. H. Shih, Q. Zheng, N.-C. Yen, C. C. Tung, and H. H. Liu, "The empirical mode decomposition and the Hilbert spectrum for nonlinear and non-stationary time series analysis", Proc. R. Soc. Lond. A **454**, 903 (1998).

[54] R. Fossion, G. Torres Vargas, and J. C. López Vieyra, "Random-matrix spectra as a time series", Phys. Rev. E **88**, 060902 (2013).

[55] N. E. Huang and Z. Wu, "A review on Hilbert–Huang transform: method and its applications to geophysical studies", Rev. Geophys. **46** (2008) 10.1029/2007RG000228.

[56] N. E. Huang and S. S. P. Shen, *Hilbert–Huang transform and its applications*, Vol. 5, Interdisciplinary Mathematical Sciences (World Scientific Publishing Company, 2005).

[57] Z. Wu and N. E. Huang, "Ensemble empirical mode decomposition: a noise-assisted data analysis method", Adv. Adapt. Data. Anal. **01**, 1 (2009).

[58] M. E. Torres, M. A. Colominas, G. Schlotthauer, and P. Flandrin, "A complete ensemble empirical mode decomposition with adaptive noise", in IEEE international conference on acoustics, speech and signal processing (ICASSP) (2011), p. 4144.

[59] M. A. Colominas, G. Schlotthauer, M. E. Torres, and P. Flandrin, "Noise-assisted EMD methods in action", Adv. Adapt. Data Anal. **04**, 1250025 (2012).

[60] M. Gaudin, "Sur la loi limite de l'éspacement des valeurs propres d'une matrice aléatoire", Nucl. Phys. **25**, 447 (1961).

[61] A. Relaño, J. M. G. Gómez, R. A. Molina, J. Retamosa, and E. Faleiro, "Quantum chaos and $1/f$ noise", Phys. Rev. Lett. **89**, 244102 (2002).

[62] E. Faleiro, J. M. G. Gómez, R. A. Molina, L. Muñoz, A. Relaño, and J. Retamosa, "Theoretical derivation of $1/f$ noise in quantum chaos", Phys. Rev. Lett. **93**, 244101 (2004).

[63] J. M. G. Gómez, A. Relaño, J. Retamosa, E. Faleiro, L. Salasnich, M. Vraničar, and M. Robnik, "$1/f^{\alpha}$ noise in spectral fluctuations of quantum systems", Phys. Rev. Lett. **94**, 084101 (2005).

[64] M. Robnik, "Classical dynamics of a family of billiards with analytic boundaries", J. Phys. A **16**, 3971 (1983).

[65] B. B. Mandelbrot, *Multifractals and* $1/f$ *noise: wild self-affinity in physics*, Selected works, Benoit B. Mandelbrot (Springer, 1999).

[66] P. Bak, C. Tang, and K. Wiesenfeld, "Self-organized criticality: an explanation of the $1/f$ noise", Phys. Rev. Lett. **59**, 381 (1987).

[67] C.-K. Peng, S. V. Buldyrev, S. Havlin, M. Simons, H. E. Stanley, and A. L. Goldberger, "Mosaic organization of DNA nucleotides", Phys. Rev. E **49**, 1685 (1994).

[68] C. Matsoukas, S. Islam, and I. Rodriguez-Iturbe, "Detrended fluctuation analysis of rainfall and streamflow time series", J. Geophys. Res. **105**, 29165 (2000).

[69] E. Räsänen, O. Pulkkinen, T. Virtanen, M. Zollner, and H. Hennig, "Fluctuations of hi-hat timing and dynamics in a virtuoso drum track of a popular music recording", PLoS ONE **10**, e0127902 (2015).

[70] M. S. Santhanam, J. N. Bandyopadhyay, and D. Angom, "Quantum spectrum as a time series: fluctuation measures", Phys. Rev. E **73**, 015201 (2006).

[71] G. H. Golub and H. A. van der Vorst, "Eigenvalue computation in the 20th century", J. Comput. Appl. Math. **123**, 35 (2000).

[72] C. Lanczos, "An iteration method for the solution of the eigenvalue problem of linear differential and integral operators", J. Res. Natl. Bur. Stand. **45**, 255 (1950).

[73] (a) E. Vergini and M. Saraceno, "Calculation by scaling of highly excited states of billiards", Phys. Rev. E **52**, 2204 (1995); (b) M. A. M. de Aguiar, "Eigenvalues and eigenfunctions of billiards in a constant magnetic field", ibid. **53**, 4555 (1996); (c) A. Barnett and A. Hassell, "Fast computation of high-frequency Dirichlet eigenmodes via spectral flow of the interior Neumann-to-Dirichlet map", Comm. Pure Appl. Math. **67**, 351 (2014).

[74] R. Kosloff and H. Tal-Ezer, "A direct relaxation method for calculating eigenfunctions and eigenvalues of the Schrödinger equation on a grid", Chem. Phys. Lett. **127**, 223 (1986).

[75] M. D. Feit, J. A. Fleck, Jr., and A. Steiger, "Solution of the Schrödinger equation by a spectral method", J. Comput. Phys. **47**, 412 (1982).

[76] I. C. F. Ipsen, "Computing an eigenvector with inverse iteration", SIAM Rev. **39**, 254 (1997).

[77] R. I. McLachlan and G. R. W. Quispel, "Splitting methods", Acta Numerica **11**, 341 (2002).

[78] (a) H. F. Baker, "Alternants and continuous groups", Proc. London Math. Soc. **s2-3**, 24 (1905); (b) J. E. Campbell, "On a law of combination of operators (second paper)", ibid. **s1-29**, 14 (1897); (c) F. Hausdorff, "Die symbolische Exponentialformel in der Gruppentheorie", Ber. Verh. Kgl. Sächs. Ges. Wiss. Leipzig **58**, 19 (1906); (d) E. B. Dynkin, "Calculation of the coefficients in the Campbell–Hausdorff formula", Dokl. Akad. Nauk SSSR **57**, (in Russian), 323 (1947); (e) W. Magnus, "On the exponential solution of differential equations for a linear operator", Commun. Pure Appl. Math. **7**, 649 (1954); (f) M. Weyrauch and D. Scholz, "Computing the Baker–Campbell–Hausdorff series and the Zassenhaus product", Comput. Phys. Commun. **180**, 1558 (2009).

[79] Q. Sheng, "Solving linear partial differential equations by exponential splitting", IMA J. Numer. Anal. **9**, 199 (1989).

[80] M. Suzuki, "General theory of fractal path integrals with applications to many-body theories and statistical physics", J. Math. Phys. **32**, 400 (1991).

[81] (a) M. Suzuki, "Hybrid exponential product formulas for unbounded operators with possible applications to Monte Carlo simulations", Phys. Lett. A **201**, 425 (1995); (b) S. A. Chin, "Symplectic integrators from composite operator factorizations", ibid. **226**, 344 (1997).

[82] (a) A. D. Bandrauk and H. Shen, "Improved exponential split operator method for solving the time-dependent Schrödinger equation", Chem. Phys. Lett. **176**, 428 (1991); (b) A. D. Bandrauk, E. Dehghanian, and H. Lu, "Complex integration steps in decomposition of quantum exponential evolution operators", ibid. **419**, 346 (2006).

[83] (a) S. A. Chin, "Multi-product splitting and Runge–Kutta–Nyström integrators", Celest. Mech. Dyn. Astron. **106**, 391 (2010); (b) S. Blanes, F. Casas, and J. Ros, "Extrapolation of symplectic integrators", ibid. **75**, 149 (1999).

[84] S. A. Chin, S. Janecek, and E. Krotscheck, "An arbitrary order diffusion algorithm for solving Schrödinger equations", Comput. Phys Commun. **180**, 1700 (2009).

[85] M. Aichinger, S. A. Chin, and E. Krotscheck, "Fourth-order algorithms for solving local Schrödinger equations in a strong magnetic field", Comput. Phys. Commun. **171**, 197 (2005).

[86] S. Janecek and E. Krotscheck, "Gauge-invariant real-space method for density functional calculations in an external magnetic field", Phys. Rev. B **77**, 245115 (2008).

[87] T. Helgaker, M. Jaszuński, and K. Ruud, "Ab initio methods for the calculation of NMR shielding and indirect spin-spin coupling constants", Chem. Rev. **99**, 293 (1999).

[88] P.-O. Löwdin, "Quantum theory of cohesive properties of solids", Adv. Phys. **5**, 1 (1956).

[89] M. Aichinger and E. Krotscheck, "A fast configuration space method for solving local Kohn–Sham equations", Comput. Mater. Sci. **34**, 188 (2005).

[90] L. Lehtovaara, J. Toivanen, and J. Eloranta, "Solution of time-independent Schrödinger equation by the imaginary time propagation method", J. Comput. Phys. **221**, 148 (2007).

[91] B. C. Carlson and J. M. Keller, "Orthogonalization procedures and the localization of Wannier functions", Phys. Rev. **105**, 102 (1957).

[92] W. Kohn, "Nobel Lecture: electronic structure of matter – wave functions and density functionals", Rev. Mod. Phys. **71**, 1253 (1999).

[93] (a) E. Runge and E. K. U. Gross, "Density-functional theory for time-dependent systems", Phys. Rev. Lett. **52**, 997 (1984); (b) C. A. Ullrich, *Time-dependent density-functional theory: concepts and applications* (Oxford University Press, 2012).

[94] P. Hohenberg and W. Kohn, "Inhomogeneous electron gas", Phys. Rev. **136**, B864 (1964).

[95] W. Kohn and L. J. Sham, "Self-consistent equations including exchange and correlation effects", Phys. Rev. **140**, A1133 (1965).

[96] C. Attaccalite, S. Moroni, P. Gori-Giorgi, and G. B. Bachelet, "Correlation energy and spin polarization in the 2D electron gas", Phys. Rev. Lett. **88**, 256601 (2002).

[97] J. P. Perdew and Y. Wang, "Accurate and simple analytic representation of the electron-gas correlation energy", Phys. Rev. B **45**, 13244 (1992).

[98] U. von Barth, "Basic density-functional theory – an overview", Physica Scripta **2004**, 9 (2004).

[99] E. J. Heller, "Bound-state eigenfunctions of classically chaotic Hamiltonian systems: scars of periodic orbits", Phys. Rev. Lett. **53**, 1515 (1984).

[100] L. Kaplan, "Scars in quantum chaotic wavefunctions", Nonlinearity **12**, R1 (1999).

[101] (a) A. I. Shnirelman, "Ergodic properties of eigenfunctions", Uspekhi Mat. Nauk **29**, (in Russian), 181 (1974); (b) S. Zelditch, "Uniform distribution of eigenfunctions on compact hyperbolic surfaces", Duke Math. J. **55**, 919 (1987); (c) Y. Colin de Verdiere, "Ergodicité et fonctions propres du laplacien", Commun. Math. Phys. **102**, 497 (1985).

[102] S. W. McDonald, "Wave dynamics of regular and chaotic rays", Lawrence Berkeley Laboratory Report No. LBL-14837, PhD thesis (University of California, Berkeley, 1983).

[103] S. W. McDonald and A. N. Kaufman, "Spectrum and eigenfunctions for a Hamiltonian with stochastic trajectories", Phys. Rev. Lett. **42**, 1189 (1979).

[104] L. Kaplan and E. J. Heller, "Linear and nonlinear theory of eigenfunction scars", Ann. Phys. **264**, 171 (1998).

[105] E. B. Bogomolny, "Smoothed wave functions of chaotic quantum systems", Physica D **31**, 169 (1988).

[106] M. V. Berry, "Quantum scars of classical closed orbits in phase space", Proc. R. Soc. Lond. A **423**, 219 (1989).

[107] (a) S. Sridhar, "Experimental observation of scarred eigenfunctions of chaotic microwave cavities", Phys. Rev. Lett. **67**, 785 (1991); (b) J. Stein and H.-J. Stöckmann, "Experimental determination of billiard wave functions", ibid. **68**, 2867 (1992).

[108] (a) T. M. Fromhold, P. B. Wilkinson, F. W. Sheard, L. Eaves, J. Miao, and G. Edwards, "Manifestations of classical chaos in the energy level spectrum of a quantum well", Phys. Rev. Lett. **75**, 1142 (1995); (b) P. B. Wilkinson, T. M. Fromhold, L. Eaves, F. W. Sheard, N. Miura, and T. Takamasu, "Observation of 'scarred' wavefunctions in a quantum well with chaotic electron dynamics", Nature **380**, 608 (1996); (c) E. E. Narimanov and A. D. Stone, "Origin of strong scarring of wave functions in quantum wells in a tilted magnetic field", Phys. Rev. Lett. **80**, 49 (1998).

[109] (a) S.-B. Lee, J.-H. Lee, J.-S. Chang, H.-J. Moon, S. W. Kim, and K. An, "Observation of scarred modes in asymmetrically deformed microcylinder lasers", Phys. Rev. Lett. **88**, 033903 (2002); (b) T. Harayama, T. Fukushima, P. Davis, P. O. Vaccaro, T. Miyasaka, T. Nishimura, and T. Aida, "Lasing on scar modes in fully chaotic microcavities", Phys. Rev. E **67**, 015207 (2003).

[110] D. Wintgen and A. Hönig, "Irregular wave functions of a hydrogen atom in a uniform magnetic field", Phys. Rev. Lett. **63**, 1467 (1989).

[111] L. Huang, Y.-C. Lai, D. K. Ferry, S. M. Goodnick, and R. Akis, "Relativistic quantum scars", Phys. Rev. Lett. **103**, 054101 (2009).

[112] J. Larson, B. M. Anderson, and A. Altland, "Chaos-driven dynamics in spin-orbit-coupled atomic gases", Phys. Rev. A **87**, 013624 (2013).

[113] P. O'Connor, J. Gehlen, and E. J. Heller, "Properties of random superpositions of plane waves", Phys. Rev. Lett. **58**, 1296 (1987).

[114] (a) P. Bellomo and T. Uzer, "State scarring by "ghosts" of periodic orbits", Phys. Rev. E **50**, 1886 (1994); (b) "Quantum scars and classical ghosts", Phys. Rev. A **51**, 1669 (1995).

[115] D. Biswas, "Closed almost-periodic orbits in semiclassical quantization of generic polygons", Phys. Rev. E **61**, 5129 (2000).

[116] (a) M. Kuś, F. Haake, and D. Delande, "Prebifurcation periodic ghost orbits in semiclassical quantization", Phys. Rev. Lett. **71**, 2167 (1993); (b) B. Sundaram and R. Scharf, "A standard perspective on ghosts", Physica D **83**, 257 (1995).

[117] T. Utzmeier, P. A. Postigo, J. Tamayo, R. García, and F. Briones, "Transition from self-organized InSb quantum-dots to quantum dashes", Appl. Phys. Lett. **69**, 2674 (1996).

[118] S. M. Reimann and M. Manninen, "Electronic structure of quantum dots", Rev. Mod. Phys. **74**, 1283 (2002).

[119] P. Bakshi, D. A. Broido, and K. Kempa, "Spontaneous polarization of electrons in quantum dashes", J. Appl. Phys. **70**, 5150 (1991).

[120] S. P. Guo, H. Ohno, A. Shen, F. Matsukura, and Y. Ohno, "InAs self-organized quantum dashes grown on GaAs (211)B", Appl. Phys. Lett. **70**, 2738 (1997).

[121] M. H. Devoret and H. Grabert, "Introduction to single-charge tunneling", in *Single charge tunneling: Coulomb blockade phenomena in nanostructures*, Vol. 294, edited by H. Grabert and M. H. Devoret, NATO ASI Series B (Plenum Press, New York, 1992) Chap. 1.

[122] M. A. Kastner, "Artificial atoms", Phys. Today **46**, 24 (1993).

[123] L. P. Kouwenhoven, N. C. Van der Vaart, A. T. Johnson, W. Kool, C. J. P. M. Harmans, J. G. Williamson, A. A. M. Staring, and C. T. Foxon, "Single electron charging effects in semiconductor quantum dots", Z. Phys. B **85**, 367 (1991).

[124] P. L. McEuen, E. B. Foxman, U. Meirav, M. A. Kastner, Y. Meir, N. S. Wingreen, and S. J. Wind, "Transport spectroscopy of a Coulomb island in the quantum Hall regime", Phys. Rev. Lett. **66**, 1926 (1991).

[125] M. Macucci, K. Hess, and G. J. Iafrate, "Numerical simulation of shell-filling effects in circular quantum dots", Phys. Rev. B **55**, R4879 (1997).

[126] E. Räsänen, H. Saarikoski, V. N. Stavrou, A. Harju, M. J. Puska, and R. M. Nieminen, "Electronic structure of rectangular quantum dots", Phys. Rev. B **67**, 235307 (2003).

[127] M. A. L. Marques, A. Castro, G. F. Bertsch, and A. Rubio, "Octopus: a first-principles tool for excited electron–ion dynamics", Comput. Phys Commun. **151**, 60 (2003).

[128] J. A. Nelder and R. Mead, "A simplex method for function minimization", Comput. J. **7**, 308 (1965).

[129] T. E. Oliphant, "Python for scientific computing", Comput. Sci. Eng. **9**, 10 (2007).

[130] L. Dagum and R. Menon, "OpenMP: an industry standard API for shared-memory programming", Comput. Sci. Eng. **5**, 46 (1998).

[131] A. Stathopoulos and J. R. McCombs, "PRIMME: PReconditioned Iterative MultiMethod Eigensolver: Methods and software description", ACM Trans. Math. Softw. **37**, 21 (2010).

[132] V. Hernandez, J. E. Roman, and V. Vidal, "SLEPc: a scalable and flexible toolkit for the solution of eigenvalue problems", ACM Trans. Math. Softw. **31**, 351 (2005).

[133] D. E. Knuth, "Structured programming with go to statements", ACM Comput. Surv. **6**, 261 (1974).

[134] V. Kotimäki, E. Räsänen, H. Hennig, and E. J. Heller, "Fractal dynamics in chaotic quantum transport", Phys. Rev. E **88**, 022913 (2013).

[135] M. Galassi, J. Davies, J. Theiler, B. Gough, G. Jungman, P. Alken, M. Booth, and F. Rossi, *GNU Scientific Library reference manual* (Network Theory Limited, UK, 2009).

[136] N. E. Huang, Z. Shen, and S. R. Long, "A new view of nonlinear water waves: the Hilbert spectrum", Annu. Rev. Fluid. Mech. **31**, 417 (1999).

[137] T. E. Oliphant, "Python for scientific computing", Comput. Sci. Eng. **9**, 10 (2007).

[138] D. Kim and H.-S. Oh, "EMD: a package for empirical mode decomposition and Hilbert spectrum", R J. **1**, 40 (2009).

[139] D. C. Bowman and J. M. Lees, *The Hilbert-Huang transform: tools and methods*, R version 3.1.0 (2014).

[140] E. Räsänen, J. Könemann, R. J. Haug, M. J. Puska, and R. M. Nieminen, "Impurity effects in quantum dots: Toward quantitative modeling", Phys. Rev. B **70**, 115308 (2004).

[141] H. Goldstein, *Classical mechanics*, 2nd ed. (Addison-Wesley, 1980).

[142] S. Blanes and P. C. Moan, "Practical symplectic partitioned Runge–Kutta and Runge–Kutta–Nyström methods", J. Comput. Appl. Math. **142**, 313–330 (2002).

[143] A. S. Davydov, *Quantum mechanics*, 2nd ed. (Pergamon Press, 1976).

[144] C. C. Liu, T. H. Lu, Y. F. Chen, and K. F. Huang, "Wave functions with localizations on classical periodic orbits in weakly perturbed quantum billiards", Phys. Rev. E **74**, 046214 (2006).

[145] S.-Y. Lee, S. Rim, J.-W. Ryu, T.-Y. Kwon, M. Choi, and C.-M. Kim, "Ray and wave dynamical properties of a spiral-shaped dielectric microcavity", J. Phys. A **41**, 275102 (2008).

[146] H. Cao and J. Wiersig, "Dielectric microcavities: Model systems for wave chaos and non-Hermitian physics", Rev. Mod. Phys. **87**, 61 (2015).

[147] G. D. Chern, H. E. Tureci, A. D. Stone, R. K. Chang, M. Kneissl, and N. M. Johnson, "Unidirectional lasing from ingan multiple-quantum-well spiral-shaped micropillars", Appl. Phys. Lett. **83**, 1710 (2003).

[148] (a) S.-Y. Lee, S. Rim, J.-W. Ryu, T.-Y. Kwon, M. Choi, and C.-M. Kim, "Quasiscarred resonances in a spiral-shaped microcavity", Phys. Rev. Lett. **93**, 164102 (2004); (b) J. Lee, S. Rim, J. Cho, and C.-M. Kim, "Resonances near the classical separatrix of a weakly deformed circular microcavity", ibid. **101**, 064101 (2008).

[149] C.-M. Kim, S. H. Lee, K. R. Oh, and J. H. Kim, "Experimental verification of quasiscarred resonance mode", Appl. Phys. Lett. **94**, 231120 (2009).

[150] (a) E. G. Altmann, G. D. Magno, and M. Hentschel, "Non-Hamiltonian dynamics in optical microcavities resulting from wave-inspired corrections to geometric optics", Europhys. Lett. **84**, 10008 (2008); (b) N. B. Rex, H. E. Tureci, H. G. L. Schwefel, R. K. Chang, and A. D. Stone, "Fresnel filtering in lasing emission from scarred modes of wave-chaotic optical resonators", Phys. Rev. Lett **88**, 094102 (2002).

[151] W. Li, L. E. Reichl, and B. Wu, "Quantum chaos in a ripple billiard", Phys. Rev. E **65**, 056220 (2002).